



HAL
open science

An Investigation of the Active Tectonics IN Central-EASTERN MAINLAND Greece with Imaging and Decomposition of Topographic and Aeromagnetic Data

Andreas Tzanis, Haralambos Kranis, Stylianos Chailas

► **To cite this version:**

Andreas Tzanis, Haralambos Kranis, Stylianos Chailas. An Investigation of the Active Tectonics IN Central-EASTERN MAINLAND Greece with Imaging and Decomposition of Topographic and Aeromagnetic Data. *Journal of Geodynamics*, 2010, 49 (2), pp.55. 10.1016/j.jog.2009.09.042. hal-00608931

HAL Id: hal-00608931

<https://hal.science/hal-00608931>

Submitted on 16 Jul 2011

HAL is a multi-disciplinary open access archive for the deposit and dissemination of scientific research documents, whether they are published or not. The documents may come from teaching and research institutions in France or abroad, or from public or private research centers.

L'archive ouverte pluridisciplinaire **HAL**, est destinée au dépôt et à la diffusion de documents scientifiques de niveau recherche, publiés ou non, émanant des établissements d'enseignement et de recherche français ou étrangers, des laboratoires publics ou privés.

Accepted Manuscript

Title: An Investigation of the Active Tectonics IN Central-EASTERN MAINLAND Greece with Imaging and Decomposition of Topographic and Aeromagnetic Data

Authors: Andreas Tzanis, Haralambos Kranis, Stylianos Chailas



PII: S0264-3707(09)00109-4
DOI: doi:10.1016/j.jog.2009.09.042
Reference: GEOD 936

To appear in: *Journal of Geodynamics*

Received date: 19-1-2009
Revised date: 17-9-2009
Accepted date: 21-9-2009

Please cite this article as: Tzanis, A., Kranis, H., Chailas, S., An Investigation of the Active Tectonics IN Central-EASTERN MAINLAND Greece with Imaging and Decomposition of Topographic and Aeromagnetic Data, *Journal of Geodynamics* (2008), doi:10.1016/j.jog.2009.09.042

This is a PDF file of an unedited manuscript that has been accepted for publication. As a service to our customers we are providing this early version of the manuscript. The manuscript will undergo copyediting, typesetting, and review of the resulting proof before it is published in its final form. Please note that during the production process errors may be discovered which could affect the content, and all legal disclaimers that apply to the journal pertain.

**AN INVESTIGATION OF THE ACTIVE TECTONICS
IN CENTRAL-EASTERN MAINLAND GREECE
WITH IMAGING AND DECOMPOSITION
OF TOPOGRAPHIC AND AEROMAGNETIC DATA**

Andreas Tzani¹

*Department of Geophysics – Geothermy, University of Athens,
Panepistimiopoli, 15784 Zografou, Greece, E-mail: atzani@geol.uoa.gr,*

Haralambos Kranis,

*Department of Dynamic and Applied Geology, University of Athens,
Panepistimiopoli, 15784 Zografou, Greece, E-mail: hkranis@geol.uoa.gr*

and

Stylios Chailas

*Department of Geophysics – Geothermy, University of Athens,
Panepistimiopoli, 15784 Zografou, Greece, E-mail: schailas@geol.uoa.gr*

¹ Corresponding author

ABSTRACT

We report the results of a joint analysis of aeromagnetic, topographic and tectonic data in Central-Eastern mainland Greece. The emphasis of the analysis is placed on the detection of coherent lineations (discontinuities), collocated and correlated with faulting structures detected by geological field observation. To this effect, edge detection and image enhancement was applied to digital aeromagnetic anomaly maps and digital elevation models, comprising bidirectional differentiation, wavelet transformation (imaging) and spatial decomposition/ reconstruction in the wavenumber domain. The analysis facilitated the detection of significant topographic lineaments with NNE-SSW, ENE-WSW and ESE-WNW orientations. Respectively, the aeromagnetic data exhibit two families of significant NE-SW, and one family of ESE-WNW lineaments. The major aeromagnetic and topographic lineaments coincide and have comparable width scales of the order of 2-3 km, indicating that they are produced by significant discontinuities in the upper crust. The kinematics of the NE-SW faults varies between oblique-slip and strike-slip. These faults affect Neogene to Late Quaternary deposits and have been responsible for the formation of transverse depressions and horsts. This is also corroborated by focal plane solutions from small earthquakes recorded by local networks. The nature of these structures is not yet clear. However, they have been detected by diverse methodologies, they have considerable extent and are apparently active. These attributes suggest that they may possibly be related to the propagation and diffusion of the North Anatolian and North Aegean Fault systems into the Greek mainland.

Keywords: Active tectonics, central Greece, wavelet decomposition, digital elevation model, aeromagnetic data

1 1 INTRODUCTION

2 It is a piece of trivial knowledge, that tectonic activity imprints the surface of the earth
3 with discontinuities detectable by direct observation and/ or by the analysis of digital eleva-
4 tion models or aerial and satellite images. It is also common, more or less, knowledge that the
5 total intensity magnetic anomaly maps capture the static distribution of geological units that
6 contain ferromagnetic minerals and are permanently or inductively magnetized in the Earth's
7 main magnetic field. This distribution can be determined with conventional analysis methods
8 designed to extract the geometry and magnetic properties of the structures producing the
9 anomalies.

10 Tectonic activity may also imprint magnetized geological bodies with analogous disconti-
11 nities, detectable with similar analysis methods. This is possible because faulting processes
12 will rupture such formations and dislocate the dissected blocks, "shearing" the local field and
13 producing lateral gradients in the total field intensity. Moreover, they initiate secondary proc-
14 esses that destroy the magnetic susceptibility and remanent magnetization by creating secon-
15 dary permeability that allows water to infiltrate and chemically alter the fragmented material
16 in and around fault zones. Notably, when fault slip (dislocation) is small, the latter mechanism
17 is more prominent, producing elongate "ridges" and "valleys" in the total intensity map. The
18 location of the fault would, then, be indicated by the "valley" structures. Finally, the inter-
19 faces between magnetic and non-magnetic geological formations brought together by tectonic
20 movements are evident by abrupt lateral changes in the intensity of the magnetic field. To
21 summarize, tectonic processes might result in elongate discontinuities (lineaments) in the
22 static magnetic field, which should be collocated and correlated with fault scarps detectable
23 by the analysis of digital topographic models and direct field observations. It is thus possible
24 to use aeromagnetic data as a tool of locating traces of buried faulting structures.

25 Herein, we apply these ideas to the study of central – eastern mainland Greece, in the hope
26 of deriving further insights and constraints on the active tectonic modes of the study area. Ac-
27 tive tectonics, particularly when it is complex, shapes the topographic and magnetic land-

1 scapes over a broad range of scales, from the local to the regional. For instance, the surface
2 expression of a fault or fault zone, which may change rapidly with respect to position, can be
3 a local scale feature. Broad units such as horst and graben belong to the opposite end of the
4 scale spectrum (regional). The distribution of scales is fractal and their superposition creates a
5 complex of features with spatial characteristics that may vary considerably with respect to lo-
6 cation. Thus, while some long(er) wavelength features are more or less easily discernible, the
7 short(er) wavelength lineaments are not. From the analyst's point of view things are worse
8 when the topographic or magnetic landscape is controlled by the superposition of complex,
9 past and contemporary tectonic modes. Fault scarps and fault zones are relatively long and
10 narrow and can easily be distorted by interlacing with neighbouring sub-parallel or transverse
11 features and buried in the long wavelength topographic or magnetic background. As a result,
12 their position and effects on the landscape (lineaments) are not always straightforward to ob-
13 serve. The interfering landscape elements and scales must be separated or removed, a feat fea-
14 sible with edge detection and spatial filtering methods of analysis.

15 The most frequently used edge detection methods (gradient directional filters, embossing
16 filters, differential filters) in combination with directional illumination are usually effective in
17 determining *local* gradient changes, even in complex landscapes. However, they cannot proc-
18 ess and isolate the scale of changes, neither decompose the available information into compo-
19 nents with particular spatial characteristics, which would facilitate scrutiny and appraisal of
20 their relative importance. Yet, such facilities would be very welcome tools when trying to
21 make sense out of very complex landscapes, as in the study area.

22 When faced with such problems, one must turn to less known but more effective methods
23 of analysis. Herein we use biderictional differentiation, two-dimensional wavelet imaging and
24 two-dimensional K-space (wavenumber) filtering, adapted from the F-K filtering methods of
25 petroleum geophysics. These are duly presented in Section 3. To the best of our knowledge,
26 some of these techniques (for instance K-space filtering) have not been hitherto applied to the
27 analysis of landscapes, but have proven to be very powerful and effective tools.

1 2 GEOLOGY AND TECTONICS

2 The area of central – eastern mainland Greece (Figure 1) is underlain by extensive forma-
3 tions of iron-rich (magnetic) rocks. Specifically, these comprise: (a) the ultramafic and vol-
4 canic components of the ophiolite complex in Mt Kallidromon and Mt Knimis and the
5 "schist-chert formation" to the south of Mt Chlomon; (b) the volcanic and iron-enriched com-
6 ponents of the Permo-Triassic volcano-sedimentary complex at the base of the Sub-
7 pelagonian Platform (south of Atalanti and in the area of Melidoni); (c) the quaternary volcan-
8 ics of the northern Gulf of Evia (at Lichades, Agios Konstantinos and Kamena Vourla).

9 Moreover, this is a tectonically active and unusually intricate realm, apparently hosting a
10 number of different faults, faulting zones and tectogenic structures that forge the topography,
11 and leave diverse, frequently intense and occasionally impressive imprints on the terrain. In a
12 nutshell, the tectonic fabric of our study area comprises (Figure 1):

13 Major, range-bounding E-W to ESE-WNW faults and fault zones: These are the best-
14 known structures that control the succession of horsts and graben in the area, such as the
15 North Gulf of Evia, the Lokris and the Voiotikos Kifissos basins. Representative structures of
16 this category are the Atalanti fault zone, the Arkitsa – Agios Konstantinos – Kamena Vourla
17 coastal fault system and the Kallidromon fault zone in the mainland Greece and the Telethron
18 and Kandilion Faults, which mark the north-eastern margin of the North Gulf of Evia.

19 The western part of the southern margin of the North Gulf of Evia is largely controlled by
20 the Arkitsa – Agios Konstantinos – Kamena Vourla fault system, which comprises three fault
21 zones: two of them, the eastern and western ones (Arkitsa-Longos (AF) and Kamena Vourla
22 (KVF) fault zones, respectively) strike E-W and consist of fault segments with lengths from
23 3-8 km, arranged en echelon or relay. These two fault zones are linked by the NW-SE Agios
24 Konstantinos fault (AKF). The reason why we did not consider these three structures to be a
25 single fault zone is that, although they have common kinematic characteristics, their geometry
26 is clearly different: the slip vectors measured on the fresh slickensides of all three are almost
27 invariably oriented N-NNW (340-360° –Kranis, 1999), but the strike and dip of the fault
28 planes differs significantly in the NW-SE Agios Konstantinos fault, whose fault surface has

1 quite low dip values (~ 30). To the west of this fault system extends the Molos fault zone,
2 which comprises two overlapping, right-stepping ESE-WNW segments; this is quite less pro-
3 nounced because it develops on the soft Neogene sediments of the Lokris Basin.

4 The only fault zone along the southern margin of the North Gulf of Evia related to impor-
5 tant recent earthquake events is the Atalanti fault zone (Ata), which strikes ESE-WNW and
6 consists of three segments (Ganas et al., 1998; Palyvos, 2001; Pantosti et al., 2001). The total
7 length of the Atalanti FZ is ~ 35 km. There have been no reports on direct measurements of
8 kinematic indicators, however, Skuphos (1894) reported that the superficial breaks of the
9 1894 earthquakes included a left-lateral component.

10 The northern margin of the Gulf is controlled mainly by two fault zones, the Telethron and
11 Kandilion Faults, a large part of which develops offshore; hence the absence of first-hand data
12 on their geometry and kinematics. The relationship between these two structures is currently a
13 matter of investigation.

14 The Kallidromon fault zone (Kal) is a ~ 33 km-long structure and consists of two segments.
15 It apparently is less active than the coastal fault zones (Jackson, 1999; Kranis, 1999). The
16 kinematics of this fault is not as well defined, as in the aforementioned structures. Neverthe-
17 less, Kranis (1999) indicated that it is also oblique-normal, but with opposite shear sense
18 (right-lateral strike slip component). Another conspicuous structure is the Parnassos fault,
19 which is a reactivated alpine thrust surface, having acted until at least the middle Quaternary
20 as a low-angle normal fault (Kranis and Papanikolaou, 2001).

21 A second set of recognizable (and mapable) structures are NE-SW transverse faults and
22 fault zones, located at the tips of, or within transfer zones, between the E-W neotectonic struc-
23 tures. The most prominent cases are the following:

24 (i) The Bralos – Oiti or Bralos-Pavliani fault zone (BrOe), located between Mts Kallidro-
25 mon and Oiti, at the onshore SW-prolongation of the Oreoi straits. The lithology in the area
26 does not favour direct field observations, as the fault zone crosses mud-rich flysch. Nonethe-
27 less, there are some isolated fault exposures, as in the case of the Skamnos segment which has
28 a ENE-WSW strike and bears striations that indicate oblique sinistral offset. Moreover, the

1 drainage pattern of the Assopos river, which develops along the trace of this zone, indicates
2 strong tectonic influence through NE-SW zones (Kranis, 1999, 2002). This fault zone can also
3 be associated with the 1983 six-month earthquake swarm located in the vicinity of Pavliani
4 (Burton et al., 1995; Kranis, 2002).

5 (ii) The Hyambolis – Hya – fault zone (Palyvos, 2001; Kranis et al., 2001): it has been
6 mapped along the western and northwestern margins of Mt Chlomo and consists of E-W to
7 ENE-WSW-trending left-stepping en echelon segments. The Profitis Elias Sfakas horst, lo-
8 cated at the SW portion of the zone is a prominent feature of the deformation zone (located
9 along a restraining bend of it) and is clearly discernible in all topographic and aeromagnetic
10 analyses performed within the scope of this study. This structure seems to play an important
11 role, acting as a barrier (albeit not clearly active) on the western tip of the ESE-WNW Ata-
12 lanti fault zone, which does not extend further west, into the Lokris basin.

13 (iii) The Malesina (Ma) fault zone: this active structure (it ruptured in the 1894 earth-
14 quakes, see Pantosti et al., 2001 for discussion) has an overall NE-SW trend, is linked with
15 the Atalanti fault zone (and most probably affects its segmentation) and controls the morphol-
16 ogy of the Malesina peninsula. However, unlike the previous two NE-SW fault zones, which
17 can be characterized as oblique-slip, this one is more typical of a normal fault, with character-
18 istic footwall back-tilt (Palyvos, 2001), although no directly measured kinematic indicators
19 have been reported.

20 The third set of recognizable structures, are NNE-SSW ($N10^{\circ}$ - 20°) lineations mapped by
21 Kranis (1999). They are found to cross the elongated ranges of Mts Knimis and Kallidromon,
22 but, with the exception of the strike-slip Melidoni fault (MF) at eastern Knimis, no kinematic
23 indicators have been found, nor has their activity been confirmed. A characteristic example is
24 the Lihades fault (Li), which straddles Mt Knimis and seems to have facilitated the intrusion
25 of the Lihades and Agios Konstantinos Upper Quaternary volcanics. Another one, found a
26 few km west of it, is the Voagrios structure (Vo), which dissects Mt Kallidromon in two.
27 Kranis (1999) noted that there are two major lineations that straddle the entire central-eastern

1 mainland Greece (the Lihades-Antikyra and the Molos – Itea Lineaments), the nature of
2 which remains unclear.

3

4 3 DATA ANALYSIS

5 The topographic and aeromagnetic data used in this study comprise a digital elevation
6 model (DEM) and digital aeromagnetic anomaly model (DAAM).

7 The DEM is shown in Figure 2a and was constructed from high resolution scanned images
8 of the 1:50,000 scale topographic maps, compiled by the Hellenic Army Geographical Survey
9 (HAGS). The images were digitized along contour lines and the digitized coordinates were
10 transformed to the Hellenic Geographical Reference System (HGRS-87). The total field
11 DAAM is shown in Figure 2b and was created by digitizing the 1:50,000 residual anomaly
12 aeromagnetic contour maps obtained from the Institute of Geological and Mining Research
13 (IGME) and originally compiled by Hunting Geology and Geophysics Ltd. These maps were
14 originally prepared so as to comply with the existing HAGS sheets. They were also digitized
15 along contour lines and transformed to the HGRS-87. The Hunting maps were measured at a
16 nominal flight altitude of 300m A.G.L, with measurement spacing along flight lines ≤ 250 m
17 and mean distance between flight lines ≈ 800 m. This affords a resolution of 250m at best. Ac-
18 cordingly, we have interpolated the digitized contours onto a 250m x 250m HGRS-87 grid.
19 The adopted digitization procedure allows a resolution as fine as the nominal error in the hori-
20 zontal direction. For the elevation data this is as small as ± 10 m and much finer than the reso-
21 lution afforded for the aeromagnetic data. In order to maintain a healthy tradeoff between data
22 volume and desired resolution while still being able to compare the results, the DEM was con-
23 structed by interpolating the digitized contours onto a HGRS-87 grid with 100x100m spacing.

24 The topography of the study area (and to a lesser extent the total magnetic intensity) exhib-
25 its a wide range of fractally distributed scales, from small hills and individual fault scarps to
26 broad topographic units such as the horst and graben structures of the Kallidromon and Oiti
27 mountain chains on the mainland and the Gulf of Evia respectively. Since more than one con-

1 temporary faulting directions are known to exist (and more have existed in the past), the spec-
2 trum and interference of the different topographic scales creates a complex pattern (noise) that
3 may obscure many important linear features produced by the tectonic activity. Thus, while
4 some long(er) wavelength features (e.g. small horsts and graben such as is the Profitis Elias
5 Sfakas horst) are more or less easily discernible, the short(er) wavelength lineaments are not.
6 We attempt to remove the interference and bring out the important linear features using the
7 methods of analysis described forthwith.

8

9 3.1 Spatial differentiation.

10 One robust and almost always dependable edge detection method is spatial differentiation,
11 which eliminates long wavelength, slowly varying elements and enhances local, short wave-
12 length changes, such as for instance fault scarps. Herein, we use double partial differentiation
13 in mutually orthogonal directions. In operational form this can be written as

$$14 \quad D_{xy}T = \frac{\partial}{\partial y} \left(\frac{\partial T}{\partial x} \right), \quad (1)$$

15 where (x) is the equatorial and (y) is the meridional direction (or vice versa), and where T
16 represents the DEM. The result of this operation (equivalent to a second order derivative) will
17 show the spatial structure of the lateral rate of change in the topography, which according to
18 the above discussion may indicate the position, orientation and size of faulting structures and
19 lateral discontinuities. Moreover, it will attenuate trends almost exactly parallel to the (x) and
20 (y) axes, thus eliminating clutter from linear elements with N-S and E-W orientations. This is
21 a not undesirable side-effect, since our main objective is to study the NE-SW and NW-SE
22 lineaments related to contemporary tectonics. It is also noted that such a sequence of differen-
23 tiations may produce random noise at an angle of 45°; to suppress this effect the data is
24 smoothed by convolving it with a diagonal 3-point Hamming filter.

25

1 3.2 Wavelet imaging

2 Edge detection can also be done with wavelet transformation (imaging), in combination
 3 with multi-scale analysis of the data. The wavelet transform can decompose a spatial data se-
 4 ries into a spectrum of energy levels at given wavelength bands and given locations. In effect,
 5 the wavelet transform matches the spatial localization of the data to the wavelength of inter-
 6 est, providing fine resolution at short wavelengths and broad spatial localization at long wave-
 7 lengths. This is much more versatile and informative than the Fourier transform, which will
 8 provide the power spectrum at given wavelength bands but for the *entire* data series, smooth-
 9 ing out any wavelength-local characteristics. On a single scale the wavelet transform is a lin-
 10 ear, narrow-band filter. For multi-scale analysis the wavelet can be rescaled to longer and
 11 shorter lengths, providing a suite of different size filters, which are convolved with the data to
 12 pick out features with wavelengths matching the filters' bandwidths: small-scale events will
 13 match small wavelets but not large wavelets and vice versa. By applying the suite of filters to
 14 the spatial data it is possible to identify local (transient) characteristics, as well as distinguish
 15 features on different scales (or even identify regions where events of certain scales are miss-
 16 ing.

17 Suitable wavelets for the stated purposes (edge detection and multi-scale analysis) are lin-
 18 ear B-spline wavelets (Chui, 1992; Daubechies, 1992; Little, 1993, 1994) and the derivative
 19 of the cubic B-spline (Canny, 1986; Little, 1994). Details on B-spline wavelets can be found
 20 in Chui (1992) or Daubechies (1992) and only essential information will be given herein.

21 The one-dimensional linear B-spline wavelet is constructed from the linear B-spline func-
 22 tion

$$23 \quad N_2(x) = \begin{cases} 0 & x < 0 \\ x & 0 \leq x < 1 \\ 2-x & 1 \leq x < 2 \\ 0 & x \geq 2 \end{cases} \quad (2)$$

24 as

$$25 \quad W_2 = \frac{1}{12} [N_2(2x) - 6N_2(2x-1) + 10N_2(2x-2) - 6N_2(2x-3) + N_2(2x-4)] \quad (3)$$

1 This wavelet transforms a step edge (change of slope) of scale comparable to the length of
2 the wavelet, into a low and a high thus generating a series of contrasting peaks and valleys
3 that demarcate local topographic changes.

4 In order to demonstrate how this wavelet transforms our data and provide a measure of the
5 information to be mined with this approach, we present an example of its application on a
6 single topographic profile running along a SSW-NNE direction at the west side of the study
7 area, across the northern flanks of Mt Parnassos and through the Bralos plateau, Mt Kallidro-
8 mon and the delta of Spercheios River to the southern foothills of Mt Othrys. This series of
9 mountains and plateaus / valleys correspond to a series of horsts and graben formed by fault
10 zones with very large cumulative vertical displacements and an average NW-SE orientation.

11 Figure 3a shows the application of 20- point (middle panel) and 40-point (bottom panel)
12 linear B-spline wavelets on the topographic profile (top panel). The 20-point wavelet will pick
13 out features with widths (wavelengths) of the order of 2 km, comparable to its length, while
14 eliminating longer or shorter components. The topography is transformed into a series of
15 highs and lows demarcating the locations of steps or breaks and, to the extent that these steps
16 and breaks are produced by faults, the location of the faults. The 40-point wavelet will pick
17 out features with widths of the order of 4 km, thus providing information on topographic steps
18 and breaks of twice the width above (lower panel). Therefore, (to the extent that they are pro-
19 duced by faulting), the peaks and troughs of the considerably smoother 40-point transform
20 will correspond to broader, possibly quasi-regional fault zones, in contrast to the more local-
21 ized events brought out by the 20-point transform.

22 When the data depend on two spatial dimensions, (a matrix or image), the wavelet trans-
23 form decomposes it into a series of images, each of which contains information at a specific
24 location, of features at a single scale (wavelength). Moreover, the existence of two independ-
25 ent variables allows each wavelength to be coupled with a particular orientation. Thus, scale
26 and orientation can be varied so as to construct a matrix filter tuned for any trait in the topog-
27 raphy. It follows that the precision in location (resolution) of any feature in the wavelet trans-

1 form will depend on its scale. In our case, it will be a function of the width (primarily) and
2 length of the lineament / fault zone.

3 The two-dimensional filter is built by sidewise arranging a number of identical one-
4 dimensional wavelets to create a 2-D matrix, tapering the edge-parallel direction with a Han-
5 ning window and rotating the resulting matrix to the desired orientation. The length of the
6 one-dimensional wavelet (edge-normal direction) determines the width of the topographic
7 features to be isolated. The number of parallel wavelets (edge-parallel direction) determines
8 the feature length over which to smooth. If the edge-parallel size is large, then only very long
9 and linear features will be identified. If it is small, then both long and short (or curved) fea-
10 tures will be picked out. As an example, in Figure 3b we present a 40x30 matrix filter of lin-
11 ear B-spline wavelets arranged in a S-N direction (top left), which will detect E-W edges with
12 widths of the order of 4 km, smoothed over lengths of 3 km. The same filter rotated to N40°
13 (top right and bottom) will detect features with similar scales and orientations N40° and
14 N295°.

15

16 3.3 **K-space filtering.**

17 The DEM was also processed with a two-dimensional K-space filter in order to isolate and
18 study elements with different orientations. To the extent that topography is controlled by tec-
19 tonics, the separation of oppositely oriented topographic features removes much of the clutter
20 caused by their superposition and facilitates more clear observations of the effects of different
21 tectonic modes on the topography, and their relative importance thereof. To this effect, we
22 have implemented techniques of F-K domain filtering (borrowed from petroleum geophysics
23 and applied to the two-dimensional Fourier transforms of matrices with one temporal and one
24 spatial dimension), to the $k_x - k_y$ domain resulting from the two-dimensional Fourier transfor-
25 mation of matrices with two spatial dimensions. A good introduction to F-K techniques exists
26 in Robinson et al., (1986). It is quite straightforward, although beyond the scope of this paper,
27 to show that features with positive slope (NE-SW oriented or up-dipping in geophysical jar-
28 gon) map into the positive k_y quadrant of the $k_x - k_y$ domain, while features with negative

1 slope (NW-SE oriented or down-dipping) map into the negative k_y quadrant. Therefore, by
2 specifying a filter that stops an entire quadrant while passing the other, we can reject features
3 oriented in one direction or the other. Furthermore, in the wavenumber domain it is possible
4 to define specific pass or stop regions such, as to further isolate and process (attenuate or am-
5 plify) specific spatial sub-characters of the data for further scrutiny. In this way we can sepa-
6 rate intersecting or overlaid elements and study their interactions. For instance, it is possible
7 to see which lineaments are relatively younger or more active by studying their effect on
8 lineaments with transverse orientations.

10 3.4 Edge detection in aeromagnetic data.

11 There exist several edge detection methods with particular application to magnetic and
12 aeromagnetic data. These include the horizontal gradient method and the application of some
13 type of compass gradient filtering on the observed data grid, or on the horizontal gradient of
14 the pseudogravity transform (Blakely and Simpson, 1986), or the total gradient (e.g. Phillips,
15 1998), or on the local wavenumber (e.g. Thurston and Smith, 1997). These methods are tuned
16 to detect discontinuities and boundaries between magnetic – non-magnetic formations by de-
17 termining the direction of maximum slope of first order derivatives, or linear combinations of
18 first and second order derivatives (local wavenumber).

19 Some of these methods rely on drastic assumptions, or are very susceptible to noise. For
20 example, the method by Blakely and Simpson (1986) requires vertical contacts between mag-
21 netic and non-magnetic formations (Grauch and Cordell, 1987), while the correct calculation
22 of the pseudogravity transform calls for a quasi-homogeneous distribution of the total mag-
23 netization vector over the study area. Violation of these assumptions can result in displace-
24 ment of the contacts away (typically down dip) from their true locations (Grauch and Cordell,
25 1987). Neither one of these conditions is satisfied for our data. The distribution of the total
26 magnetization vector is both unknown and highly heterogeneous (see Section 2 for details),
27 while the tectonic (Alpine) emplacement of the main magnetic formations and their continu-
28 ous post-alpine disturbances do not guarantee the existence of upright contacts. The local

1 wavenumber method implements cascaded partial differentiations, which introduce noise
 2 unless the data is smoothed or upward continued, in which case small amplitude features are
 3 lost.

4 The 3-D analytic signal has been introduced by Nabighian (1984), who also showed by
 5 way of the generalized Hilbert transform, that the vertical and horizontal derivatives of a po-
 6 tential field are related as

$$7 \quad \mathbb{F} \left\{ \frac{\partial M}{\partial z} \right\} = -\frac{ik_x}{\sqrt{k_x^2 + k_y^2}} \cdot \mathbb{F} \left\{ \frac{\partial M}{\partial x} \right\} - \frac{ik_y}{\sqrt{k_x^2 + k_y^2}} \cdot \mathbb{F} \left\{ \frac{\partial M}{\partial y} \right\} \quad (4)$$

8 where $\mathbb{F}\{\bullet\}$ denotes the Fourier transform and M stands for the DAAM. The total gradient is,
 9 then,

$$10 \quad G = \frac{\partial M}{\partial x} \mathbf{i} + \frac{\partial M}{\partial y} \mathbf{j} + \frac{\partial M}{\partial z} \mathbf{k} . \quad (5)$$

11 The modulus of the total gradient

$$12 \quad A = \sqrt{\left(\frac{\partial M}{\partial x} \right)^2 + \left(\frac{\partial M}{\partial y} \right)^2 + \left(\frac{\partial M}{\partial z} \right)^2} \quad (6)$$

13 can be shown to peak over isolated magnetic contacts and can be used as an indicator of local
 14 changes in the DAAM (e.g. Roest et al, 1992). Because this method requires the computation
 15 of the vertical derivative by means of the Fourier transform of the horizontal derivatives, it
 16 may be somewhat more susceptible to noise than the Blakely and Simpson method. However,
 17 there is no reduction-to-the-pole transformation required (and no relevant distortion). More-
 18 over, it is not subject to the same assumptions and does not result in displaced contacts. For
 19 all the above reasons, herein we will implement the analytic signal (total gradient) method.

20

21

1 4 RESULTS AND OBSERVATIONS

2

3 4.1 Topographic lineaments and active faults

4 Figure 4a presents the topographic gradient $D_{xy}T$ of the DEM and Figure 4b is the same,
5 but with inclusion of the traces of active neotectonic faults recognized by direct field observa-
6 tion: this is the most detailed image of *local* changes in topography, afforded by this data. The
7 Figure clearly illustrates the existence of significant lineaments with NNE-SSW, NE-SW and
8 ESE-WNW orientations. The topographic gradient has higher amplitude at the location of
9 significant topographic discontinuities, given also that the magnitude of a morphological dis-
10 continuity depends on the activity (deformation rate) of a faulting structure, its kinematics and
11 the lithology: the more discernible combination is dip-slip or oblique-slip kinematics with a
12 footwall comprising hard (erosion – resistant) rocks.

13 Very good correlation between ESE-WNW of lineaments and faults can readily be ob-
14 served, as in the case of the Atalanti fault zone (Ata in Figure 1), the extensive Kallidromon
15 fault zone (Kal in Figure 1), the Arkitsa – Agios Konstantinos – Kamena Vourla coastal fault
16 system (AF – AKF – KVF in Figure 1) and the Parnassos Fault. All of the mapped range-
17 bounding faults are typical neotectonic structures for the broader Aegean region (Stewart and
18 Hancock, 1988). As stated in the introduction their kinematics deviates significantly from
19 pure dip-slip, by as much as 25% of strike-slip component. The coastal fault system is charac-
20 terized by a systematic sinistral component, evidenced by the kinematic indicators on the ex-
21 posed slickensides; the mean slip vector is N10°W and this value remains more or less con-
22 stant, in spite of strike variations of the fault segments.

23 Likewise, there is very good correlation between ENE-WSW lineaments and ENE-WSW
24 to NE-SW faults. One such significant example is the Bralos – Oiti (BrOe in Figure 1). This
25 lies in the SW-ward prolongation of the Oreoi Straits, a very narrow graben separating Evia
26 from Magnesia and Fthiotis in mainland Greece. This structure is controlled by offshore NE-
27 SW active faults (Perissoratis et al., 1991) and may well be related to propagation of the

1 North Anatolian fault zone into the North Aegean (Sengör, 1979). Other important such struc-
2 tures with characteristic signature in the topographic gradient is the Hyampolis fault zone
3 (Hya in Figure 1). Located at the W and NW margin of Mt. Chlomo, it comprises a set of E-
4 W to ENE-WSW left-stepping en-echelon blocks (such as and the Profitis Elias Sfakas horst,
5 Kranis et al., 2001), lending it a general NE-SW orientation. This structure intercepts the Ata-
6 lanti fault zone and as stated in the introduction, may be responsible for the dramatic diminu-
7 tion of its cumulative vertical offset. A third important and seismically active NE-SW struc-
8 ture is the Malesina fault zone, (Ma in Figure 1); this may also affect the Atalanti fault zone,
9 which it intercepts at the area of Martino. It is also possible to observe a SW-ward prolonga-
10 tion of the feature, which coincides with an ENE-WSW fault at the footwall of the Atalanti
11 fault zone but with *opposite* polarity (dip). It is, thus, difficult to talk about a direct WSW ex-
12 tension of Malesina fault zone, across the footwall of the Atalanti fault zone. Even so, as seen
13 in Figure 4, these two fault zones appear to disrupt and discontinue the ESE-WNW normal
14 faults.

15 Wavelet imaging was applied on the basis of the observations facilitated by Figure 4. Fig-
16 ures 5a and 5b respectively show the transforms resulting from a 20x20 matrix wavelet (reso-
17 lution 2x2 km) and a 40x40 matrix wavelet (resolution 4x4 km), both oriented at N20° and
18 roughly perpendicular to the dominant ESE-WNW lineaments of the topographic gradient. To
19 increase image readability, only the positive peaks of the wavelet transforms are shown. The
20 existence of linear, coherent ESE-WNW changes in the terrain slope is immediately apparent.
21 These correlate remarkably with the mapped traces of the range-bounding fault zones having
22 corresponding orientation. Again, particular attention is drawn to the Ata, Kal, AF and Par-
23 nassos fault zones. The correlation between faults and topographic lineaments observed at the
24 resolution level of grid spacing (Figure 4), is shown to persist at increasingly larger scales.
25 Accordingly, the fault zones producing these lineaments can be recognized as major land-
26 scape shaping factors. Additional, significant linear topographic changes can be observed in
27 Figure 5b, as SE-ward prolongations of the main inland and coastal fault zones. Since these
28 are mainly observed at the larger scales, they may be associated with unmapped segments of

1 the fault zones that cannot be easily detected by field surveys, possibly because their traces
2 outcrop in softer rock and have been degraded by surface processes. Similar features can also
3 be seen in the island of Evia and are believed to have been produced by corresponding tecton-
4 ics.

5 Figures 6a and b respectively show the transforms resulting from a 20x20 and a 40x40 ma-
6 trix wavelets, both oriented at N340°, roughly perpendicular to the dominant ENE-WSW
7 lineaments of the topographic gradient. Here as well, one can observe distinct NE-SW to
8 ENE-WSW lineaments that correlate with mapped faults and fault zones, with particular ref-
9 erence to BrOe, Hya and Ma fault zones. Note however that the latter is more clearly observ-
10 able at the larger scales. It is also apparent that the correlation persists at all scales, indicating
11 that these fault zones are also very important in shaping the landscape.

12 All of the above fault zones are located at the margins of neotectonic structures. Neverthe-
13 less, we can still observe ENE-WSW faults within the neotectonic structures (neotectonic
14 blocks). Such characteristic examples are the normal oblique-slip Potamia and Liapatoremma
15 faults (P and L in Figure 1), which form a small horst within the west Lokris sub-basin (Mari-
16 olakos et al., 2001). These faults correlate well with ENE-WSW lineaments in Figures 6a and
17 6b. Note however, that these lineaments are significantly longer than the mapped lengths of
18 the faults, with particular reference to the Liapatoremma fault. This possibly implies the exis-
19 tence of faulting with a correspondingly significant scale, whose surface expressions may be
20 obscured from field observations by the dense forest, and also by their interaction with trans-
21 verse WNW-ESE and NNE-SSW structures (also see below).

22 Significant ENE-WSW lineaments can also be observed in Figures 6a and 6b, approxi-
23 mately midway between the Liapatoremma / Potamia and Hyampolis fault zones, as well as in
24 the island of Evia to the NE. In addition, very significant such topographic changes exist in
25 the area of Mt Parnassos. In fact, these appear to be a natural extension/ continuation of the
26 Hyampolis (primarily) and Malesina fault zones, hinting to the existence of a long, broad and
27 apparently important zone of faulting, disrupted only where it interacts with the transverse

1 ESE-WNW fault systems. Such a zone would be expected to comprise a cardinal component
2 of the contemporary tectonic evolution of central Greece.

3 A final observation concerns the existence of NNE-SSW faulting structures. Such elements
4 were mapped by Kranis (1999), who could not observe clear evidence of their kinematics and
5 present dynamic state, with the exception of the left-lateral strike-slip Melidoni fault zone
6 (RM), which transverses the eastern portion of Mt. Knimis, on the footwall of the Arkitsa
7 Fault

8 Other characteristic examples NNE-SSW structures are observed at larger scales (one or-
9 der of magnitude higher) These are the Lichades fault zone (Li in Figure 1), which transects
10 Mt Knimis and Mt Kallidromon and the Voagrios fault zone (Vo in Figure 1) which transects
11 Mt. Kallidromon; notably, these lineaments appear to continue southwards and can be ob-
12 served in the area of Mt. Parnassos; Kranis (1999) has coined the names Lichades – Antikyra
13 and Itea – Molos to these lineaments but did not interpret their origin and significance.

14 Finally, Figures 7a and 7b show the result of K-space dip-reject filtering on the DEM data.
15 In Figure 7a, which shows topographic elements with orientations in the 2nd and 4th quadrant
16 (NW-SE), the dominant mode of topography is visible, comprising a sub-parallel series of
17 ranges and basins, bounded by normal faults (among them Ar, Ata, Kal and Ma); wherever
18 measured these show a non-trivial sinistral strike-slip component with NNW oriented slip
19 vectors. The Kallidromon – Chlomon and Parnassos ranges are readily discernible. The for-
20 mer becomes less clearly pronounced towards ESE; this lowering of footwall elevation was
21 noted by Kranis (1999) for the Kallidromon range and was attributed by the same author to
22 block rotation, caused by activity on presumed transverse faults. By comparing the results of
23 K-space filtering of Figure 7a with these of Figure 7b, which shows topographic elements
24 with orientations in the 1st and 3rd quadrant (NE-SW), it becomes clear that the transverse
25 and/or oblique tectonic structures have played an important part in the tectonic configuration
26 of the area. One can see that there are distinct "indentations" of the range fronts. This is ap-
27 parently a secondary mode, comprising lower amplitude elements. One such example is at the
28 intersection of the Ata with Hya, where the former terminates. The Voagrios discontinuity

1 (Vo) also affects the western part of the Kallidromon mountain front. This is particularly
2 visible in Figure 7d. Another conspicuous feature is the abrupt western termination of Kal-
3 lidromon range, which coincides with the Bralos-Oiti fault zone

4 Furthermore, we extract elements with ENE-WSW (Figure 7c) and NNE-SSW (Figure 7d)
5 orientations for further scrutiny. In Figure 7c it becomes clear that the transverse structures
6 with the largest amplitude and, consequently, importance are the BrOe and the Hya. These
7 two may be the boundaries of a ~35 km-wide deforming zone between the Sperchios graben
8 and the Oreoi Straits in the north and the Malesina peninsula and Mt Chlomo in the south.
9 Figure 7d enhances some of the most elusive structures in the study area, including the Voa-
10 grios discontinuity. Another feature visible in the same figure lies approximately 10 km to the
11 west of the Voagrios discontinuity and south of the Lichades Islets, crossing Mt Knimis. This
12 structure has affected the segmentation of the coastal fault system and can be linked to the
13 volcanic intrusions which have formed the islets and also outcrop a few km west of Kamena
14 Vourla.

16 4.2 Aeromagnetic lineaments and active faults

17 Figure 8a shows the amplitude $A > 0.01$ nT/m of the total gradient of the DAAM and Fig-
18 ure 8b is the same but emphasizing the higher amplitude gradients ($A > 0.04$ nT/m). Figures
19 9a and 9b respectively show the application of 8x8 linear B-spline matrix wavelets rotated to
20 the direction $N20^\circ$ and $N330^\circ$. Note that owing to the size of grid spacing (250m), these filters
21 will pick out scales of the order of 2x2 km.

22 The gradient of the aeromagnetic data exhibits one family of significant NE-SW linea-
23 ments and one family of ESE-WNW lineaments. The major aeromagnetic and topographic
24 lineaments are found to coincide and to have comparable scales with the topographic gradient
25 lineaments, indicating that they are produced by significant discontinuities in the upper crust.

26 Specifically, very good correlation between ESE – WNW magnetic lineaments and neotec-
27 tonic faults exists in the area of Atalanti fault zone (which transects Permo-Triassic forma-
28 tions and ophiolites in the area of Tragana) as well as in the areas of Knimis and Kallidromon

1 fault zones, which are underlain by ophiolites with a particularly complex magnetic terrain.
2 Additional evidence of such lineaments are also observed at Mt Othrys where ophiolites out-
3 crop in abundance; these are evident in both Figures 8 and Figure 9a and apparently correlate
4 with topographic lineaments.

5 Strong correlations between ENE-WSW lineaments and faults are also observable in the
6 area of Malesina fault zone and its likely prolongation across the footwall of Atalanti fault
7 zone. To the south of Atalanti town, at the foothills of Mt Roda, the Permo-Triassic forma-
8 tions are characteristically bounded by faults parallel to the Atalanti fault zone and to the NE
9 by the termination of the Hyampolis fault zone. The latter can also be traced at the area of
10 Profitis Elias Sfakas (Figure 1). The SE branch of the Hyampolis fault zone is correlated with
11 a strong magnetic lineament and defines the boundary of the ophiolites (which are covered by
12 post-alpine sediments). Evidence of ENE- WSW lineaments can be observed at the SE corner
13 of the study area (apparently due to underwater sources), at the area of Lichades islands (pre-
14 sumably associated with the Quaternary volcanic activity of the area) and at Mt Othrys
15 (ophiolites). Finally, weaker evidence of ENE-WSW lineaments exist at the ophiolitic com-
16 plex of Mt. Kallidromon.

17

18 **4.3 Fault plane solutions and GPS velocity vectors and fault-slip data.**

19 Focal mechanism solutions of small to medium earthquakes can provide useful insights
20 into the deformation pattern, especially in areas such as this, where deformation is distributed.
21 Although strain is primarily released by large events, a significant part could be released ei-
22 ther aseismically, or by small earthquakes. These events account for a small amount of the to-
23 tal released strain but are helpful in bridging the strain rate deficit observed between strain
24 rates calculated from earthquake data on one hand, and SLR and GPS data on the other (Jack-
25 son et al., 1992; Clarke et al., 1998). Moreover, these data can be useful indicators as to the
26 proposed re-adjustment of fault blocks (through rotation around vertical axes, Jackson, 2002)
27 to accommodate the deformation imposed by the regional stress field.

1 Additional evidence on the dynamics and kinematics of the study area are presented in
2 Figures 10 and 11. Figure 10 illustrates the focal mechanisms of small earthquakes observed
3 by local networks and published by Hatzfeld et al. (1999). Superimposed are focal mecha-
4 nisms of the main event ($M_w=5.1$) and major aftershock ($M_w=4.4$) of the 14/10/2008 Man-
5 toudi earthquake sequence, computed by the University of Thessaloniki (Roumelioti et al,
6 2007), as well as the Harvard CMT mechanism of the 13/12/2008 $M_w=5.2$ event. Figure 11
7 displays the horizontal projections of the slip vectors of both nodal planes from the focal
8 mechanisms of Hatzfeld et al (1999), together with the GPS velocity vectors published by
9 Clarke et al. (1998) and the mean fault-slip vectors computed herein.

10 The focal mechanism solutions show mostly oblique-slip motion, with one nodal plane
11 striking NW-SE and one second nodal plane ENE-WSW. The slip vectors of the NW-SE
12 nodal plane generally point to the SE and would appear to indicate that the area is moving to
13 this direction, as is actually contended by Hatzfeld et al (1999). The slip vectors of the ENE-
14 WSW nodal planes would appear to indicate that the area is moving SW-ward, which is con-
15 sistent with the GPS observations. Most importantly, the focal plane solutions indicate that
16 the active tectonics of the study area include a NE-SW lateral component, which is parallel to
17 the ENE-WSW neotectonic faults and topographic / aeromagnetic lineaments and consistent
18 with field observations of kinematic indicators on the ENE-WSW trending faults.

19 Inversion of fault-slip data was performed, following the direct stress inversion method of
20 Angelier and Coguel (1979) and using the computer program Tectonics FP (Reiter and Acs,
21 2003). Examples of the results are shown in Figure 12. Analysis of fault-slip data has shown
22 that the coastal fault system is characterized by NNW-oriented mean slip vector ($341^\circ/51^\circ$),
23 while the mean slip vector for the whole Kallidromon f.z. is NNE ($028^\circ/60^\circ$). The resolved
24 stress tensors for the coastal fault system and Kal show that extension direction is practically
25 identical for both σ_3 and the corresponding T-axes are oriented NNE-SSW (Fig. 12) although
26 the coastal shows greater deviation between measured and calculated extension directions; the
27 latter may be indicative of multi-phase tectonics having affected the coastal fault system, a
28 notion suggested by Kranis (2007). Kranis and Papanikolaou (2001) had calculated NE-

1 oriented extension for the Parnassos Fault, based on two measurement stations, close to Am-
2 fikleia. This extension direction is compatible with the orientation of the Pliocene- Lower
3 Pleistocene extension suggested by Mercier et al. (1989), which in turn means that the Parn
4 (Parnassos fault) has ceased to operate. However, this may not be the case, as recently col-
5 lected fault-slip data from the entire Parnassos mountain front show indications of N-S to
6 NNE-SSW extension, which is compatible with the current stress field (Kranis and Skourtsos,
7 work in preparation).

8

9 5 DISCUSSION AND CONCLUSIONS

10 The central-eastern mainland Greece is part of a broad deforming zone between the west-
11 ern tip of the North Anatolian Fault (actually the North Aegean Basin) and the Kefalonia
12 right-lateral fault in western Greece (see Burchfiel, 2004 and Kiliias et al, 2008, for recent dis-
13 cussions). It comprises a suite of more or less typical rifts, such as the graben of the gulfs of
14 Corinth and Northern Evia. Its relationship with the ongoing regional geodynamic processes
15 is still a matter of investigation, as the exact mode of deformation has not yet been elucidated.
16 In their recent paper, Kiliias et al. (2008) suggest that the broader area is characterized by a
17 combination of strike-slip and extensional deformation, within an underlapping extensional
18 zone, between the North Anatolian and Kefalonia Faults.

19 Our study has investigated the detectability of well-known faulting structures with trans-
20 formations of digital aeromagnetic and topographic models. We have also tried to appraise the
21 existence of structures not readily recognized in the field and to confirm the existence of
22 transverse structures which had been detected by field surveys but with varying degrees of
23 ambiguity, due to the nature of the syn-rift deposits or alpine clastics, which do not favour the
24 preservation of fault-related structures (esp. fault surfaces and kinematic indicators) and the
25 age-old modification of the terrain by agriculture.

26 We have found that, in addition to the well-known active E-W structures, there are others,
27 transverse and/or oblique to them, which participate in the deformation of central Greece.

1 These are, primarily, NE-SW oblique- to strike-slip fault zones located at the present-day
2 transfer zones between the E-W structures. Second, there are also NNE-SSW strike-slip zones
3 that are detected on scales that range from a few km to several tens of kilometers. The latter
4 are more enigmatic; they could correspond to a set of secondary shears (P-shears), were we to
5 adopt a transtensional NE-SW stress field for the broader area. However, neither their kine-
6 matics nor their activity has been confirmed, so this suggestion cannot be easily confirmed (or
7 rejected for that matter). It is, after all, well known that even in zones with well-defined tran-
8 stensional deformation pattern, the identification of a specific structure and its placing within
9 the standard classification of shear zone components has certain limitations (Harding et al.,
10 1985).

11 We believe that together with the well-known E-W to ESE-WNW major structures, the
12 NE-SW ones shown in this study accommodate deformation which facilitates the rotation of
13 elongated blocks (Jackson, 1994; Goldsworthy et al., 2002) within a broad shear zone that in-
14 corporates significant amount of strike-slip deformation. Given that the vast majority of ki-
15 nematic indicators (fault striations, earthquake slip vectors,) deviate substantially from being
16 pure dip-slip, together with the results of GPS surveying, it is reasonable to believe that the
17 stress field in central-eastern mainland Greece is transtensional. As shown by Kahle et al
18 (2000) the rifting process in the North Gulf of Evia is controlled by a combination of normal
19 and sinistral components which is in accordance with our observations.

20 As for the NE-SW structures, they need not be active, strictly speaking; however –and this
21 has been demonstrated in the case of the Hyambolis fault zone — they may function as pas-
22 sive segment margins, controlling the segmentation of the E-W fault zones and/or facilitated
23 the break-up of the elongated fault blocks into smaller-order ones, thus reducing their overall
24 rigidity.

25 The additional constraints placed by the slip vectors of the focal mechanism solutions
26 (Hatzfeld et al., 1999) and the velocity field, as it is known from GPS surveys (Clarke et al.,
27 1998; Kahle et al., 2000; McClusky et al., 2000) come to support our suggestions for the exis-

1 tence and function of the NE-SW structures, as a clear SW-oriented movement of the area can
2 be confirmed.

3 In conclusion, the study of the NE-SW structures has shown that they correspond to shear
4 zones, either localized, or functioning at a larger (crustal) scale. The kinematics of the faults
5 identified within these structures varies between oblique-slip and strike-slip. These faults af-
6 fect Neogene to Late Quaternary deposits and have been responsible for the formation of
7 transverse depressions and horsts. Judging from the study of the smaller-scale structures, the
8 overall kinematics of these large-scale zones must be oblique-slip (Kranis et al., 2001). Cer-
9 tainly, these structures require further scrutiny at both small and large scales, before their role
10 and contribution to the contemporary tectonics of Central Greece is unequivocally recognized.
11 Nevertheless, they have been detected by diverse methodologies and have considerable ex-
12 tent, as they seem to straddle the entire central-eastern Greece and Evia. All their observed at-
13 tributes suggest that they function so as facilitate the distribution of NE-SW and may thus be
14 related to the propagation and diffusion of the North Anatolian and North Aegean Fault sys-
15 tems into the Greek mainland.

16
17

18 REFERENCES

- 19 Angelier, J. and J. Coguel, 1979. Sur une methode simple de determination des axes princi-
20 paux des contraintes pur un population des failles. C.R. Acad. Sci. Paris, D 288, 307-310.
- 21 Blakely, R. J. and R. W. Simpson, 1986. Approximating edges of source bodies from mag-
22 netic or gravity anomalies, *Geophysics*, 51(7), 1494-1498.
- 23 Burchfiel, B.C., 2004. New Technology: new geological challenges, *GSA Today*, 14, 2, 4-10.
- 24 Burton, P.W., N.S. Melis and M. Brooks, 1995: Coseismic crustal deformation on a fault zone
25 defined by microseismicity in the Pavliani area, central Greece. *Geophys. Jour. Int.*, 123,
26 16-40.
- 27 Canny, J., 1986. A Computational Approach to Edge Detection, *IEEE Transactions on Pattern*
28 *Analysis and Machine Intelligence*, 8(6), 679-698.
- 29 Chui, C.K., 1992. An introduction to wavelets, Academic Press, New York.

- 1 Clarke, P. J., Davies, R. R., England, P. C., Parsons, B., Billiris, H., Paradissis, D., Veis, G.,
2 Cross, P. A., Denys, P. H., Ashkenazi, V., Bingley, R., Kahle, H.-G., Muller, M.-V. and
3 Briole, P., 1998. Crustal strain in central Greece from repeated GPS measurements in the
4 interval 1989 – 1997, *Geophys. J. Int.*, 135, 195 – 214.
- 5 Daubechies, I., 1992. Ten lectures on Wavelets, CBMS Regional Conference Series in Ap-
6 plied Mathematics, SIAM, Philadelphia, PA, USA.
- 7 Ganas, A., G.P. Roberts and T. Memou, 1998. Segment boundaries, the 1894 ruptures and
8 strain patterns along the Atalanti Fault, central Greece, *J. Geodynamics*, 26, 461-486.
- 9 Goldsworthy, M., J. Jackson and J. Haines, 2002. The continuity of active fault systems in
10 Greece. *Geophys. J. Int.*, 148, 596-618.
- 11 Grauch, V. J. S. and L. Cordell, 1987, Limitations on determining density or magnetic
12 boundaries from the horizontal gradient of gravity or pseudogravity data, *Geophysics*,
13 52(1), 118-121.
- 14 Harding, T.P., R.C. Vierbuchen and N. Christie-Blick, 1985. Structural styles, plate-tectonic
15 settings and hydrocarbon traps of divergent (transtensional) wrench faults. In: K.T. Biddle
16 and N. Christie-Blick (Eds.): *Strike-slip deformation, Basin Formation and Sedimentation*,
17 *Soc. Econ. Paleont. And Mineral.*, 51-77.
- 18 Hatzfeld, D., Ziazia, M., Kementzetidou, D., Hatzidimitriou, P., Panagiotopoulos, D.,
19 Makropoulos, K., Papadimitriou, P., and Deschamps, A., 1999. Microseismicity and focal
20 mechanisms at the western termination of the North Anatolian Fault, and their implications
21 for continental tectonics, *Geophys. J. Int.*, 137, 891-908
- 22 Jackson, J.A., 1994. Active Tectonics of the Aegean region. *Ann. Rev. Earth Planet. Sci.*, 22,
23 239-271.
- 24 Jackson, J.A., 1999. Fault death: a perspective from actively deforming regions. *J. Struct.*
25 *Geol.*, 21, 1003-1010.
- 26 Jackson, J.A., 2002. Using Earthquakes for Continental Tectonic Geology. *Intern. Handbook*
27 *of Earthquake and Engineering Seismology*, vol. 81A, IASPEI, 491-503.
- 28 Jackson, J.A., A. Haines and W. Holt, 1992. The horizontal velocity field in the deforming
29 Aegean Sea region determined from the moment tensor of earthquakes, *J. Geophys. Res.*,
30 97, 17657-17684.
- 31 Kahle, H-G., M. Cocard, P. Yannick, A. Geiger, R. Reilinger, A. Barka and G. Veis, 2000.
32 GPS-derived strain field within the boundary of the Eurasian, African and Arabian Plates.
33 *J. Geoph. Res.*, 105, 23353-23370.

- 1 Kilias, A.A., M.D. Tranos, E.E. Papadimitriou and V.G. Karakostas, 2008. The recent crustal
2 deformation of the Hellenic orogen in Central Greece; the Kremasta and Sperchios Fault
3 Systems and their relationship with the adjacent large structural features. *Z.dr. Ges. Ge-*
4 *owiss.*, 159, 533-547
- 5 Kranis, H.D. 1999. Neotectonic activity of Fault zones in Lokris, central-eastern mainland
6 Greece (Lokris), Ph.D. Thesis, GAIA, No. 10, Univ. of Athens, 234. pp.
- 7 Kranis, H.D. and D. I. Papanikolaou, 2001. Evidence for detachment faulting on the NE Par-
8 nassos mountain front (Central Greece). *Bull. Geol. Soc. Greece*, XXXIV/1, 281-287.
- 9 Kranis, H.D., 2002. Kinematics of active faults in Lokris, central Greece – block rotation
10 within a crustal-scale shear zone? *Proc. XVII Congress of the Carpatho-Balkan Geol. Ass.*,
11 J. Michalik, L. Simon and J. Vozar (Eds), *Geologica Carpathica*, 53, 157-159.
- 12 Kranis, H.D., N. Palyvos, G. Livaditis and H. Maroukian, 2001. The Hyambolis Zone: geo-
13 morphological and tectonic evidence of a transverse structure in Lokris (Central Greece).
14 *Bull. Geol. Soc. Greece*, XXXIV/1, 251-257.
- 15 Kranis, H.D., 2007. Neotectonic basin evolution in central-eastern mainland Greece. *Proc.*
16 *11th Intern. Congress, Athens, May 2007*, *Bull. Geol. Soc. Greece*, 40, 360-373.
- 17 Little, S. A., 1994. Wavelet Analysis of Seafloor Bathymetry: An Example, in *Wavelets in*
18 *Geophysics*, Efi Foufoula-Georgiou and Praveen Kumar (eds.), Academic Press, San
19 Diego, 167-182.
- 20 Little, S. A., Carter, P. H. and Smith, D. K., 1993. Wavelet analysis of a bathymetric profile
21 reveals anomalous crust. *Geophys. Res. Lett.*, 20(18), 1915-1918.
- 22 Mariolakos, I., H. Kranis, H. Maroukian and I. Fountoulis, 2001. Tectonically controlled
23 drainage evolution in Lokris (Sterea Hellas). *Bull. Geol. Soc. Greece*, XXXIV/1, 175-182
24 (in Greek).
- 25 McClusky, S.C., Balassanian, S., Barka, A., Demir, C., Ergintav, S., Georgiev, I., Gurkan, O.,
26 Hamburger, M., Hurst, K., Kahle, H., Kastens, K., Kekelidze, G., King, R., Kotzev, V.,
27 Lenk, O., Mahmoud, S., Mishin, A., Nadariya, M., Ouzounis, A., Paradissis, D., Peter, Y.,
28 Prilepin, M., Reilinger, R., Sanli, I., Seeger, H., Tealeb, A., Toksoz, M.N., and Veis, G.,
29 2000, Global positioning system constraints on plate kinematics and dynamics in the east-
30 ern Mediterranean and Caucasus: *Journal of Geophysical Research*, 105, 5695–5719.
- 31 Mercier, J.L., D. Sorel, and P. Vergely, 1989. Extensional tectonic regimes in the Aegean ba-
32 sins during the Cenozoic. *Basin Research*, 2, 49-71.

- 1 Nabighian, M. N., 1984. Toward a three-dimensional automatic interpretation of potential
2 field data via generalized Hilbert transforms: Fundamental relations, *Geophysics*, 40(6),
3 780-786.
- 4 Palyvos, N., 2001. Geomorphological study of the broader Atalanti area (Fthiotis, Central
5 Greece), Ph.D. Thesis, Univ. of Athens, Dep. of Geology, 233 pp. (in Greek).
- 6 Pantosti, D., P.D. De Martini, D. Papanastassiou, N. Palyvos, F. Lemeille and G. Stavrakakis,
7 2001. A reappraisal of the 1894 Atalanti earthquake surface ruptures, Central Greece., *Bul.*
8 *Seis. Soc. Am.*, 91, 4. 760-780.
- 9 Perissoratis, C., I Angelopoulos, D. Mitropoulos and S. Michailidis, 1991. Surficial sediment
10 map of the Aegean Sea floor (scale 1:200,000): Pagasitikos sheet (and explanatory text).
11 I.G.M.E., Athens.
- 12 Phillips, J. D., 1998. Processing and Interpretation of Aeromagnetic Data for the Santa Cruz
13 Basin—Patagonia Mountains Area, South-Central Arizona, U.S. Geological Survey, Open-
14 File Report 02-98.
- 15 Reiter, F. and P. Acs, 2003. TectonicsFP software. <http://www.tectonicsfp.com>.
- 16 Robinson, E.A., Durrani, T.S. and Peardon, L.G., 1986. Geophysical signal processing, Pren-
17 tice Hall, London, p. 389-467.
- 18 Roest, W.R., Verhoef, Jacob, and Pilkington, Mark, 1992, Magnetic interpretation using the 3-
19 D analytic signal: *Geophysics*, v.57, no.1, p.116-125.
- 20 Roumelioti, Z., Ch. Benetatos, A. Kiratzi and D. Dreger (2007). Near-real time moment ten-
21 sors for earthquakes in Greece provided by the Dept of Geophysics, Aristotle University of
22 Thessaloniki (AUTH-solutions), Report submitted to the European Mediterranean Seis-
23 mological Center (EMSC), <http://emsc-csem.org>.
- 24 Sengör, A.M., 1979. The North Anatolian Fault: is age, offset and tectonic significance. *J.*
25 *Geol. Soc. London*, 136, 269-282.
- 26 Skuphos T., 1894. Zwei grossen Erdbeben in Lokris am 8/20 und 15/27 April, 1894.
27 *Zeitschrift Ges. Erdkunde zu Berlin*, 24, 409-474.
- 28 Stewart, S. and P. L. Hancock, 1988. Normal fault zone evolution and fault scarp degradation
29 in the Aegean region. *Basin Res.*, 1, 139-153.
- 30 Thurston, J. B. and R. S. Smith, 1997. Automatic conversion of magnetic data to depth, dip,
31 and susceptibility contrast using the SPItm method, *Geophysics*, 62(3), 807-813.

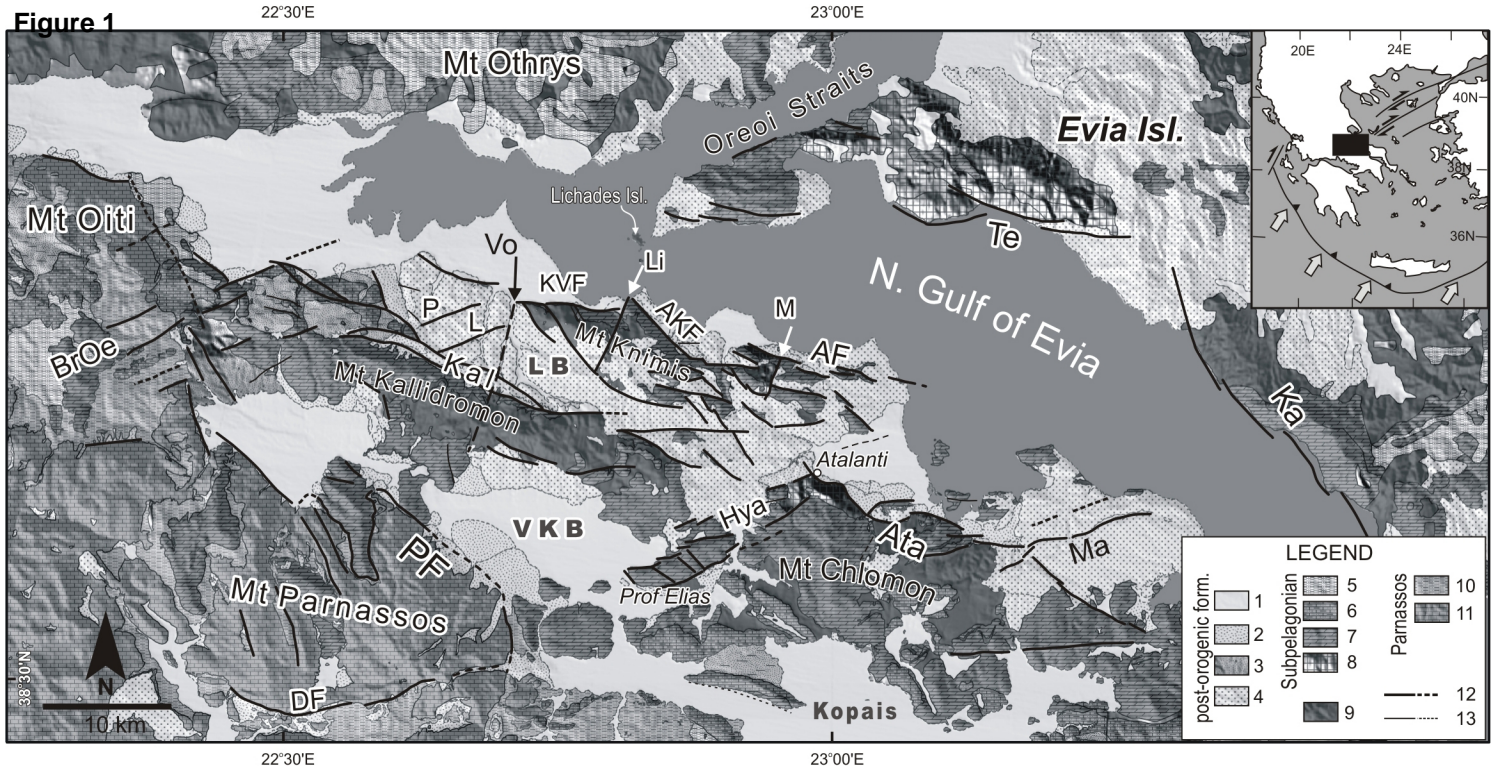
FIGURE CAPTIONS

- 1
- 2
- 3 **Figure 1.** Simplified Geological and Tectonic Map of the Study area, with the faults (F) and
- 4 fault zones (FZ) referenced in text. 1: alluvium; 2: quaternary scree; 3: Bralos for-
- 5 mation (Pleistocene); 4: Fluvio-lacustrine deposits (Pliocene-Earty Quaternary); 5:
- 6 Late Cretaceous Clastics; 6: Late Cretaceous carbonates; 7: Triassic-Jurassic car-
- 7 bonates; 8: volcanoclastic complex and Sub-Pelagonian basement; 9: ophiolite suite;
- 8 10: Parnassos Unit flysch; 11: P.U. carbonates; 12: Major faults; 13: Minor faults.
- 9 Te: Telethron FZ; Kandilion FZ; Ma: Malesina FZ; Ata:Atalanti FZ; Hya: Hyam-
- 10 polis FZ; AF: Arkitsa FZ; AKF: Agios Konstantinos FZ; KVF: Kamena Vourla FZ;
- 11 BrOe: Bralos-Oiti FZ; Ka: Kallidromon FZ; P: Potamia F; L: Liapatorrema F; Li:
- 12 Lihades F; M: Melidoni F; Vo: Voagrios F; LB: Lokris Basin; VKB: Voiotikos Ki-
- 13 fissos Basin.
- 14 **Figure 2a.** The digital elevation model of the study area (100m grid spacing).
- 15 **Figure 2b.** The digital aeromagnetic anomaly model of the study area.
- 16 **Figure 3a.** Application of 20- point (middle panel) and 40-point (bottom panel) linear B-
- 17 spline wavelets on an elevation profile (top panel).
- 18 **Figure 3b. Top left:** A 40x30 matrix filter of linear B-spline wavelets arranged in the S-N di-
- 19 rection. **To right:** The same filter rotated to N40°. **Bottom:** Three-dimensional
- 20 view of the matrix filter shown in the top right panel.
- 21 **Figure 4a.** The gradient $D_{xy}T$ of the DEM calculated with equation (1)
- 22 **Figure 4b.** The gradient $D_{xy}T$ of the DEM with the traces of active faults recognized by
- 23 Kranis (1999) and Palyvos (2001).
- 24 **Figure 5a.** Image (wavelet transform) of the DEM using a 20x20 linear B-spline matrix
- 25 wavelet oriented at N20°.
- 26 **Figure 5b.** Image of the DEM using a 40x40 linear B-spline matrix wavelet oriented at N20°.
- 27 **Figure 6a.** Image of the DEM using a 20x20 linear B-spline matrix wavelet oriented at
- 28 N340°.

- 1 **Figure 6b.** Image of the DEM using a 40x40 linear B-spline matrix wavelet oriented at
2 N340°.
- 3 **Figure 7a.** K-space filtered DEM in which only the NW-SE oriented topographic elements
4 have been retained.
- 5 **Figure 7b.** K-space filtered DEM in which only the NE-SW oriented topographic elements
6 have been retained..
- 7 **Figure 7c.** K-space filtered DEM illustrating topographic elements with exclusively ESE-
8 WNW orientations.
- 9 **Figure 7d.** K-space filtered DEM illustrating topographic elements with exclusively NNE-
10 SWW orientations.
- 11 **Figure 8a.** The total gradient A of the DAAM calculated with equation (6).
- 12 **Figure 8b.** The total gradient A of the DAAM emphasizing the higher ($A > 0.04$ nT/m) val-
13 ues.
- 14 **Figure 9a.** Image (wavelet transform) of the DAAM using an 8x8 linear B-spline matrix
15 wavelet oriented at N20°.
- 16 **Figure 9b.** Image of the DAAM using an 8x8 linear B-spline matrix wavelet oriented at
17 N330°.
- 18 **Figure 10.** Focal mechanisms of local earthquakes. The black beach balls indicate the small
19 earthquake activity observed by local networks (Hatzfeld et al., 1999). The grey
20 beach balls (AUTH) indicate the focal mechanisms computed by the University of
21 Thessaloniki (Roumelioti et al, 2007). The light-grey beach balls (HRV) indicate
22 the Harvard CMT mechanism of the 13/12/2008 event.
- 23 **Figure 11.** The small black and white arrows indicate the horizontal projections of the slip
24 vectors calculated from the focal mechanisms of Figure 10 (Hatzfeld et al, 1999).
25 The thin grey arrows indicate the GPS velocity vectors from Clarke et al, (1998).
26 The thick grey arrows indicate the fault mean fault-slip vectors, for each of the
27 fault segments described in text.
- 28 **Figure 12.** Fault-slip data and calculation of stress tensor with the method of direct inversion
29 for the coastal fault system (a) and the Kallidromon Fault Zone (b), following the
30 method of Angelier and Coguel (1979), with the use of TectonicsFP computer

1 program. Lower hemisphere, equal-area stereographic projections. Left panes
2 show fault-slip data and the calculated stress axes (σ_1 , σ_2 , σ_3), middle panes are
3 fluctuation-histograms of the deviation angles (angle between measured and cal-
4 culated slip vectors) and stress ratio R ($(\sigma_2 - \sigma_3) / (\sigma_1 - \sigma_3)$); right panes are P-T axes.
5

Accepted Manuscript



TOPOGRAPHY (m)

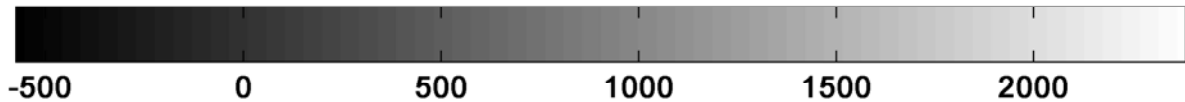
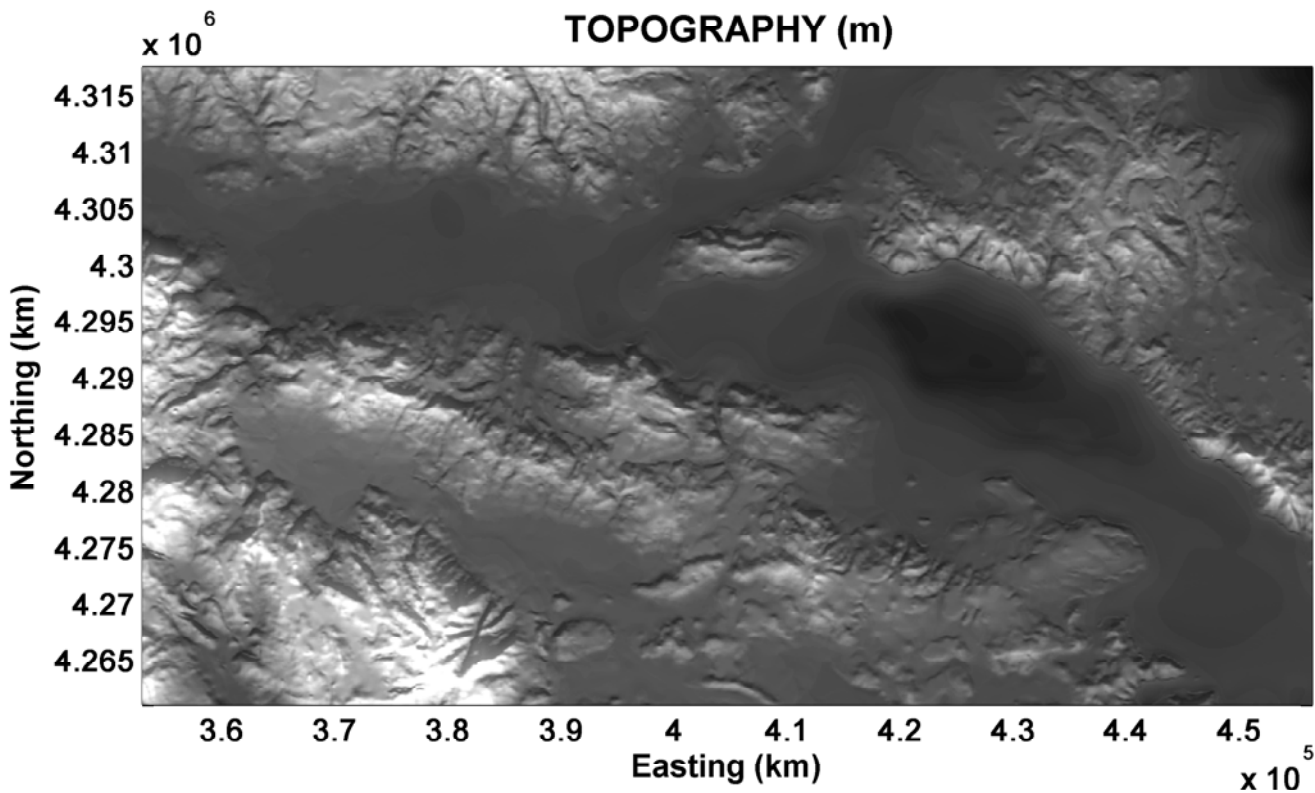
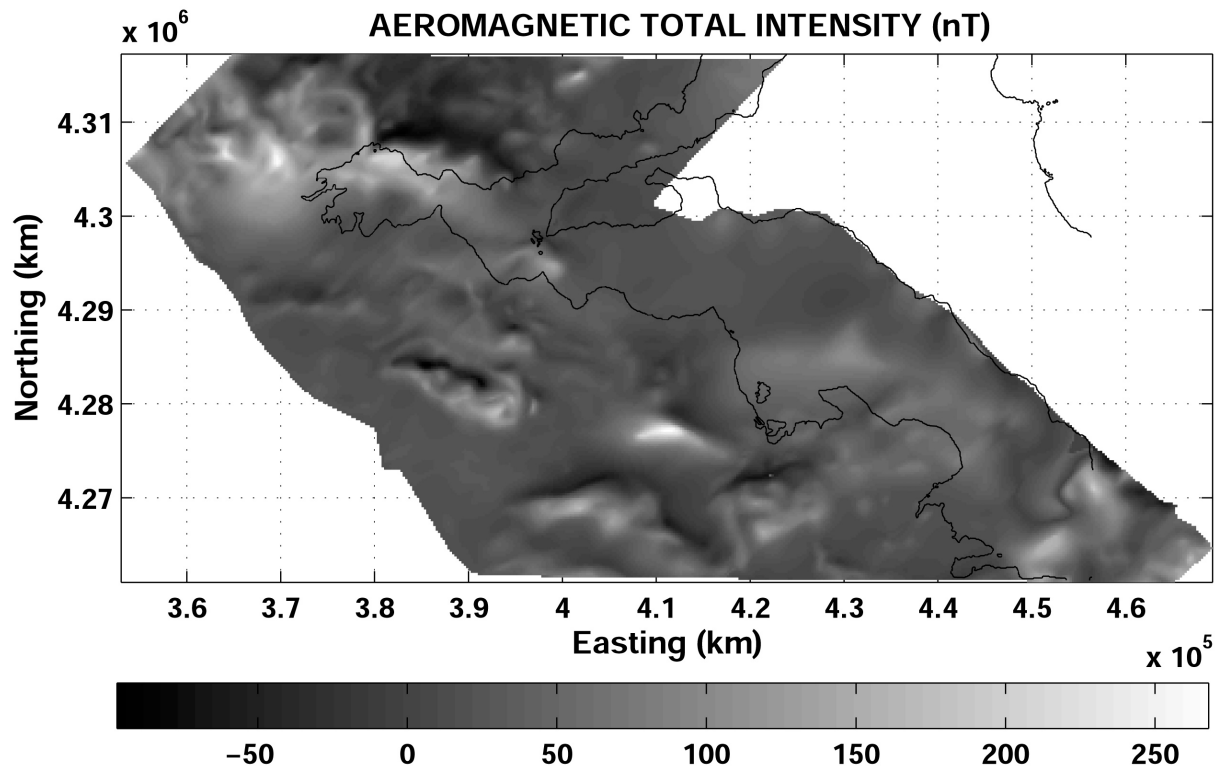
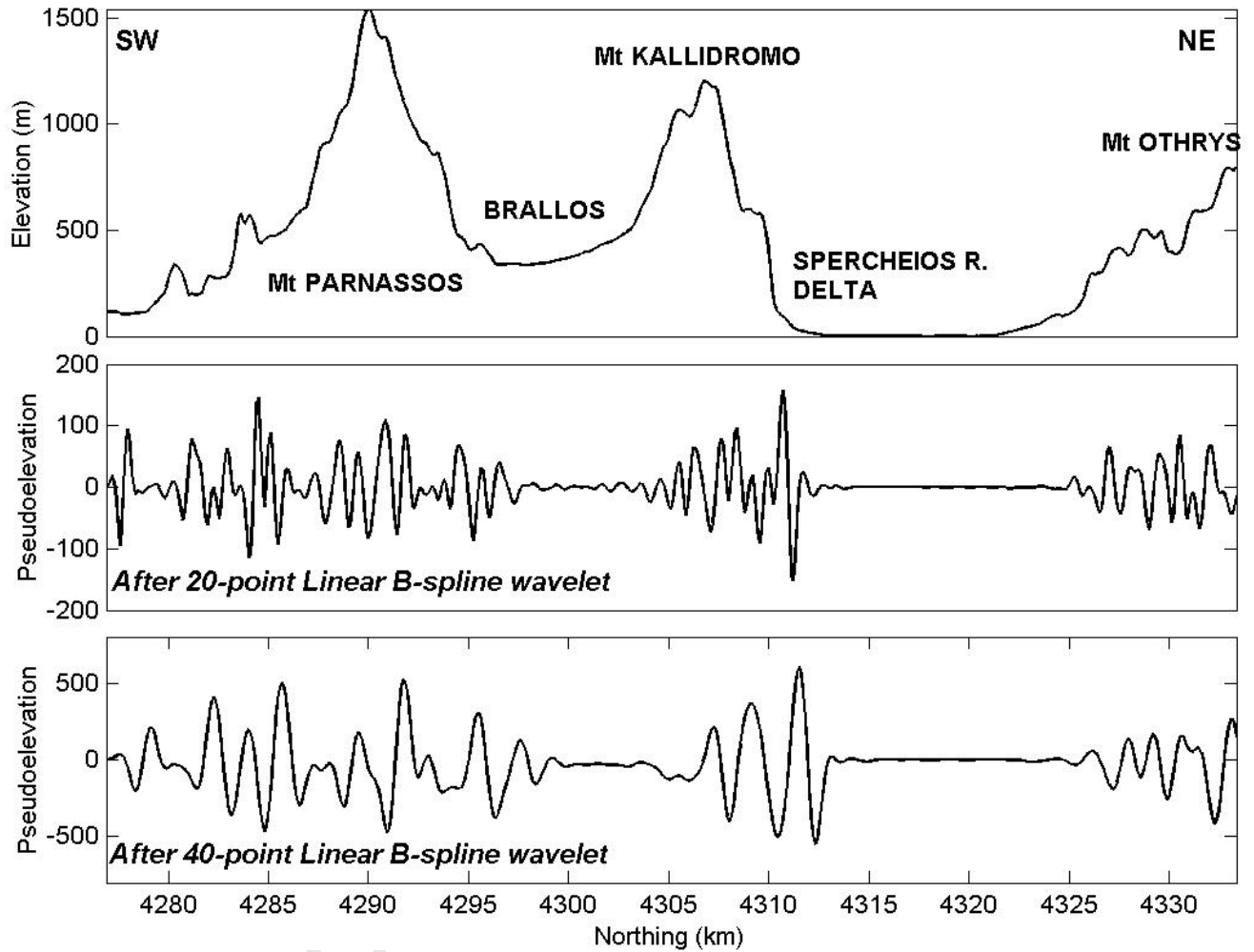
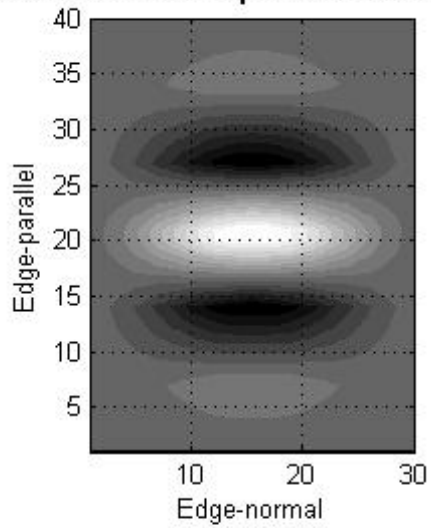
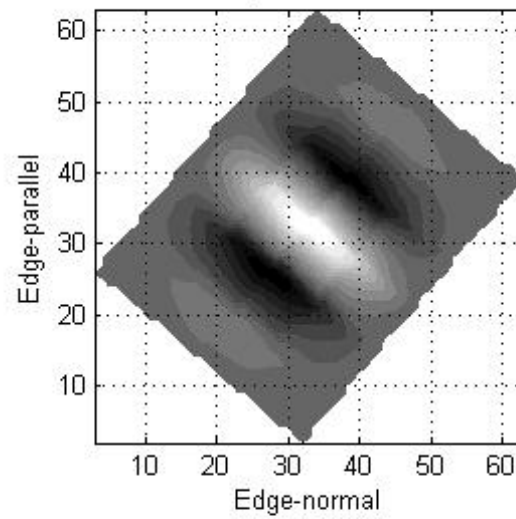
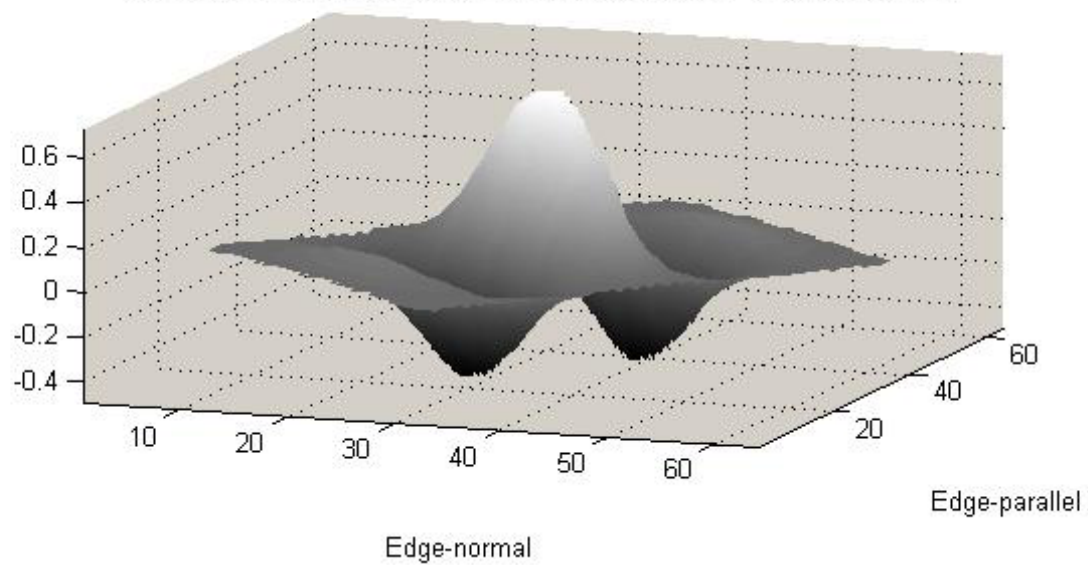
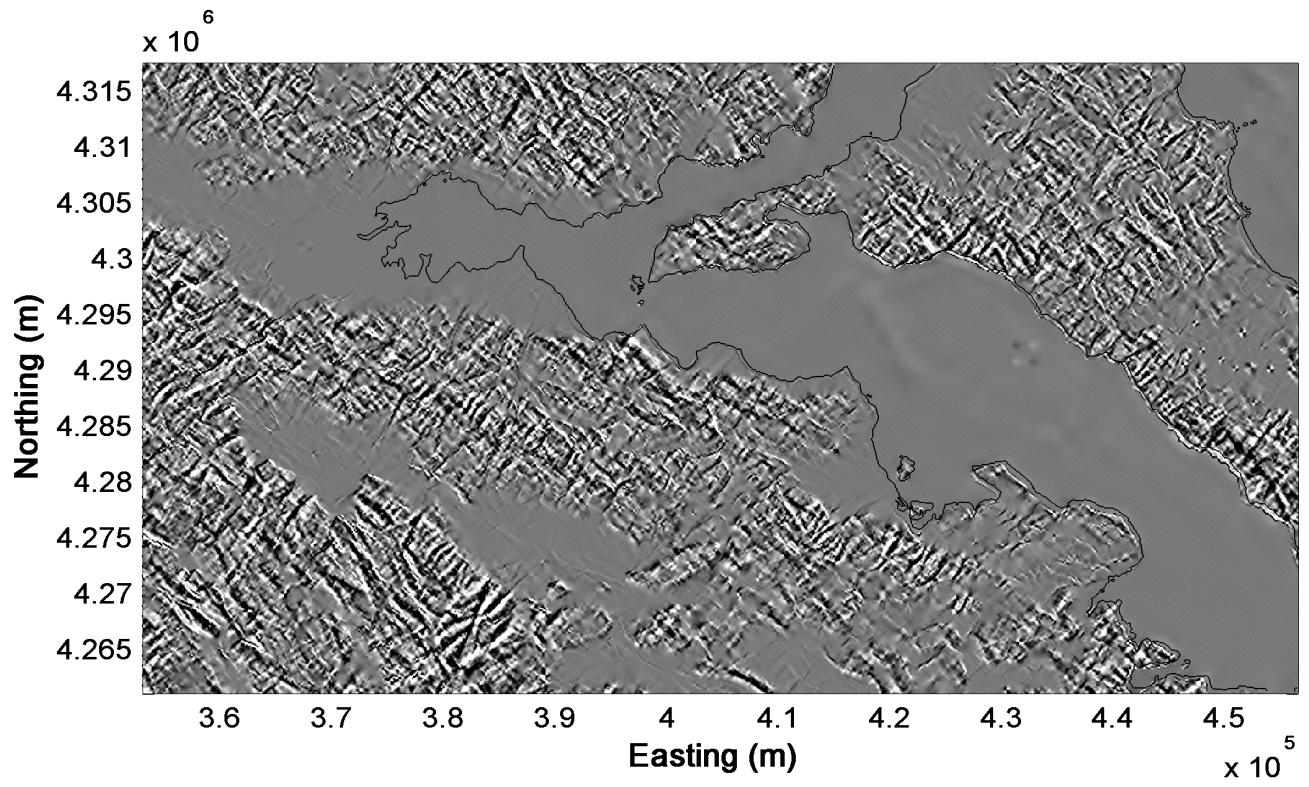


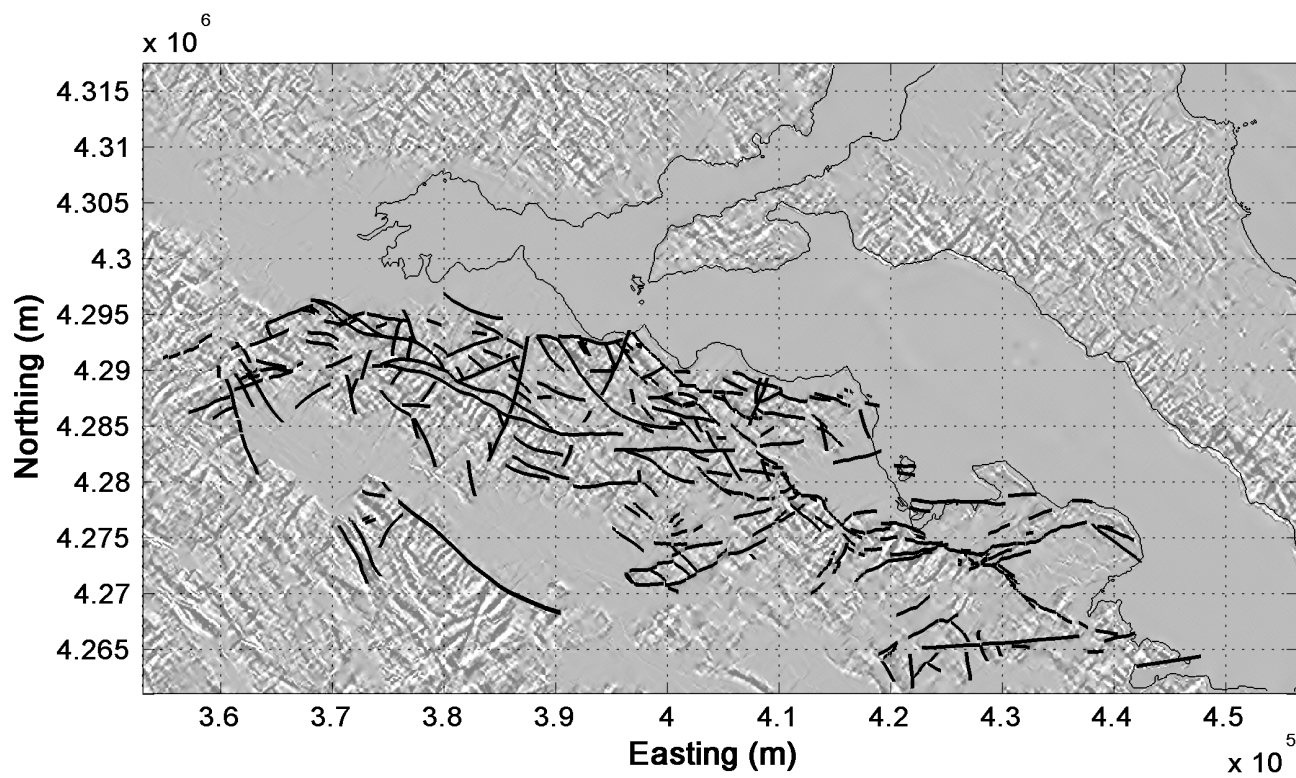
Figure 2b

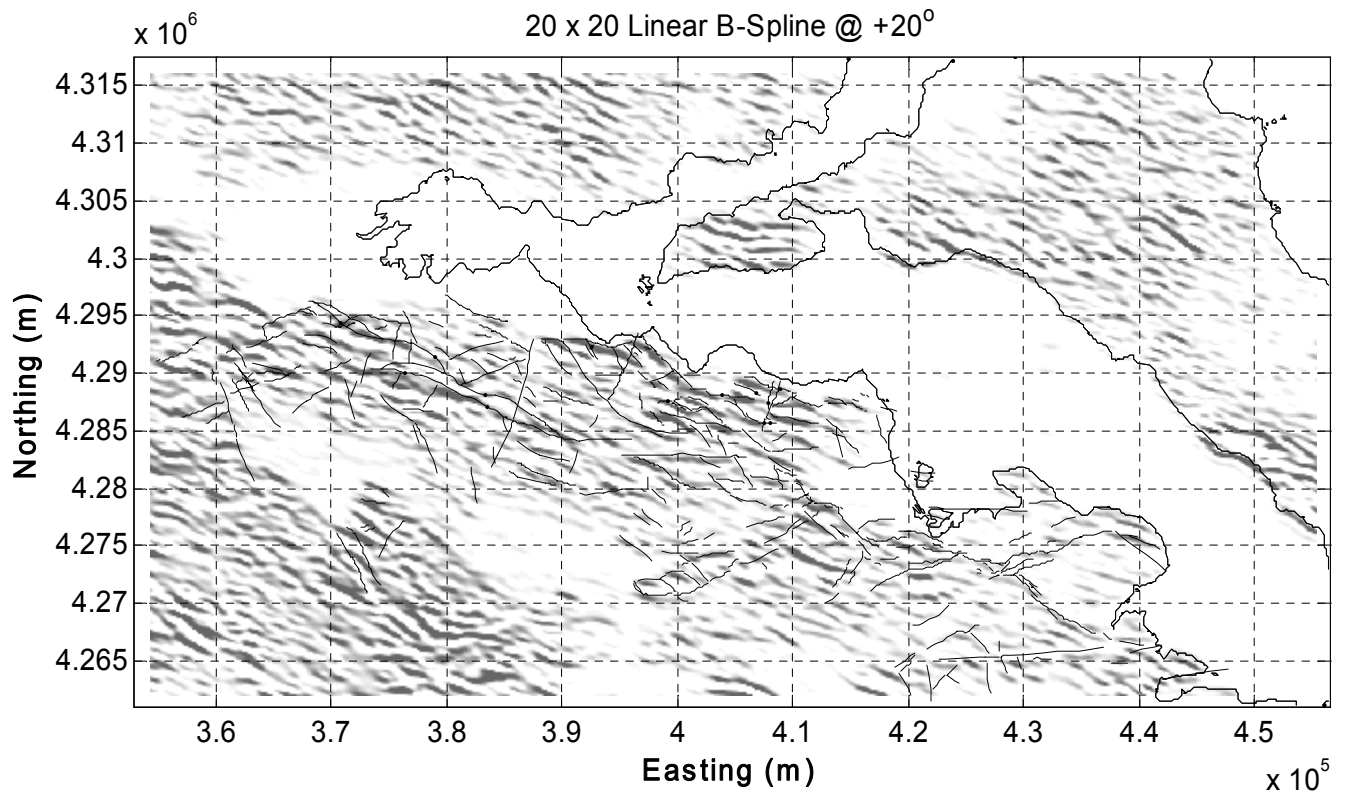




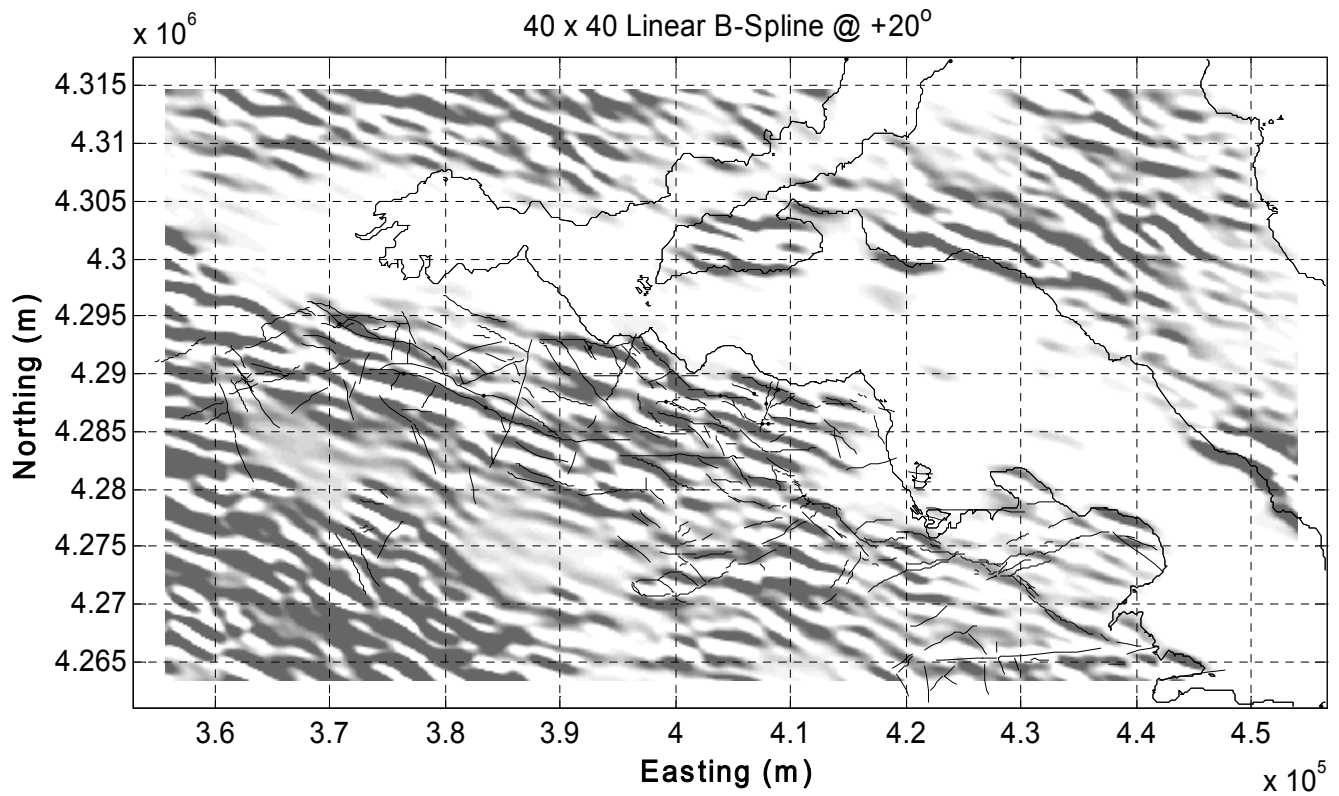
A. 40x30 Linear B-spline Matrix Wavelet**B. 40x30 Linear B-spline Matrix Wavelet @N40°****C. 40x30 Linear B-spline Matrix Wavelet @ N40° viewed from SE**



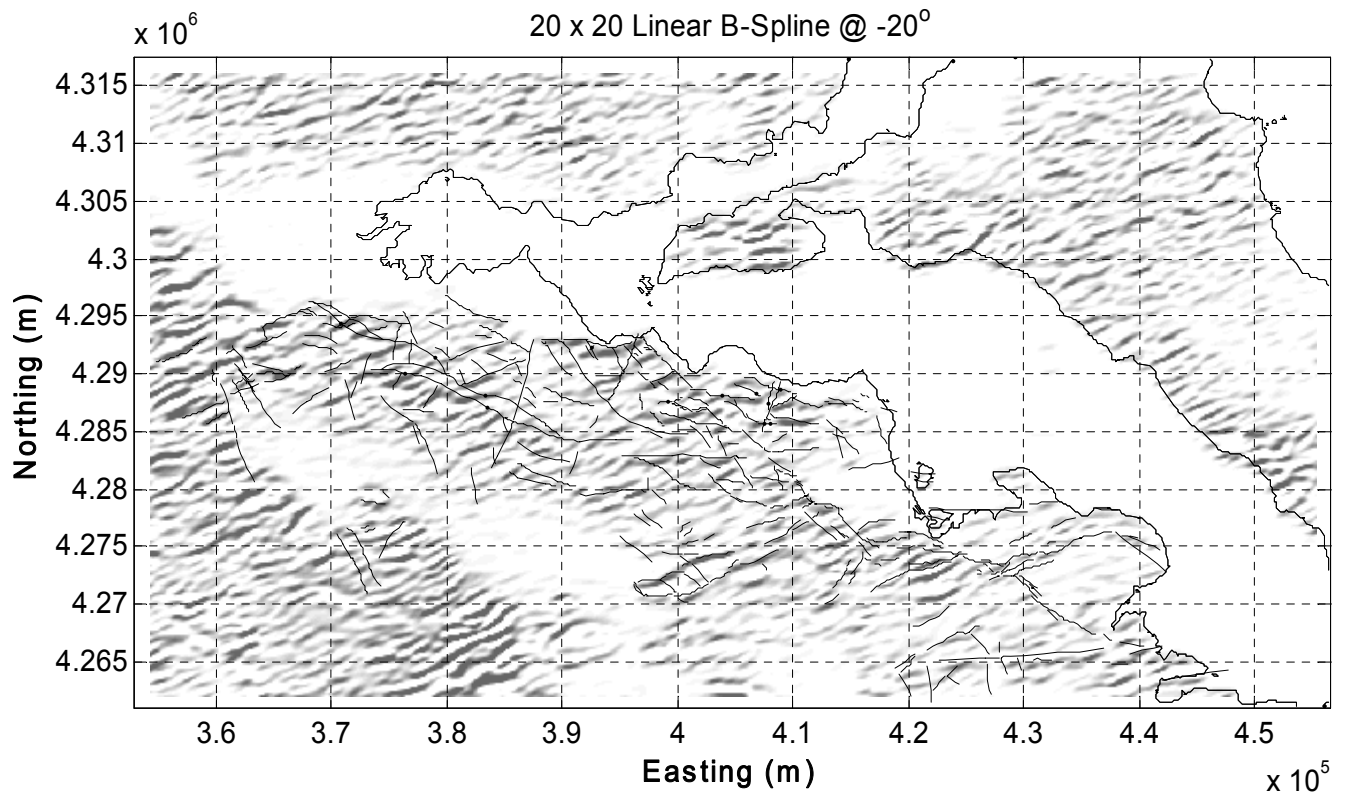




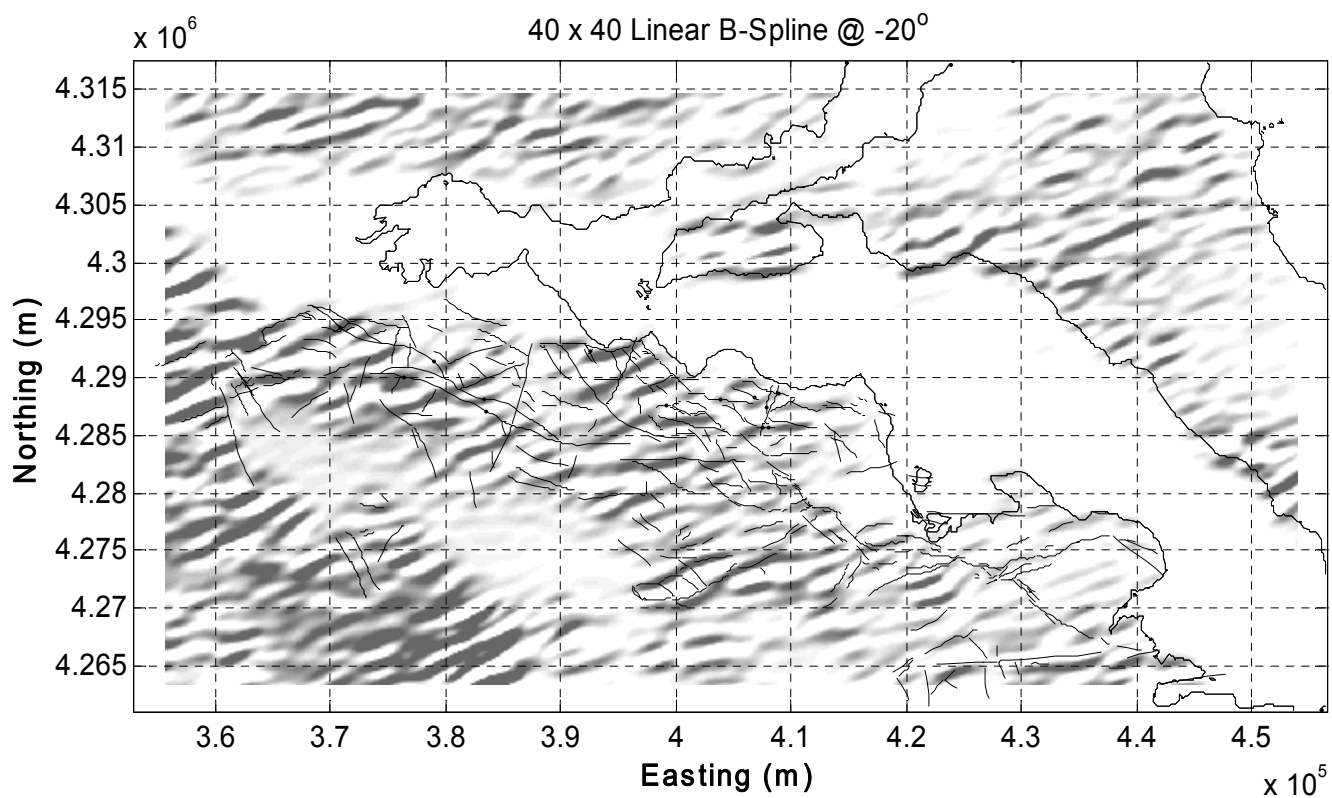
Accepte



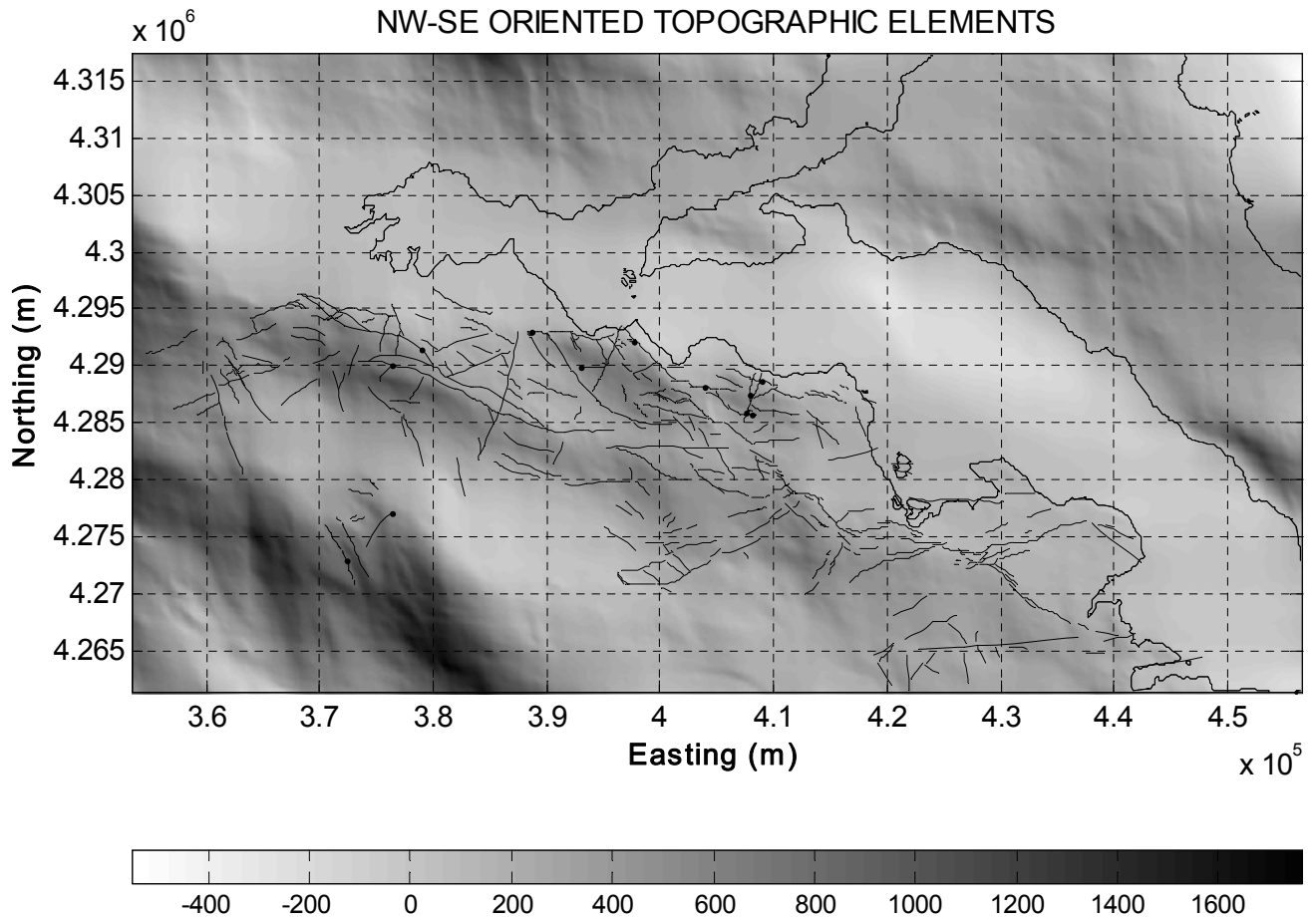
ACCEPTED

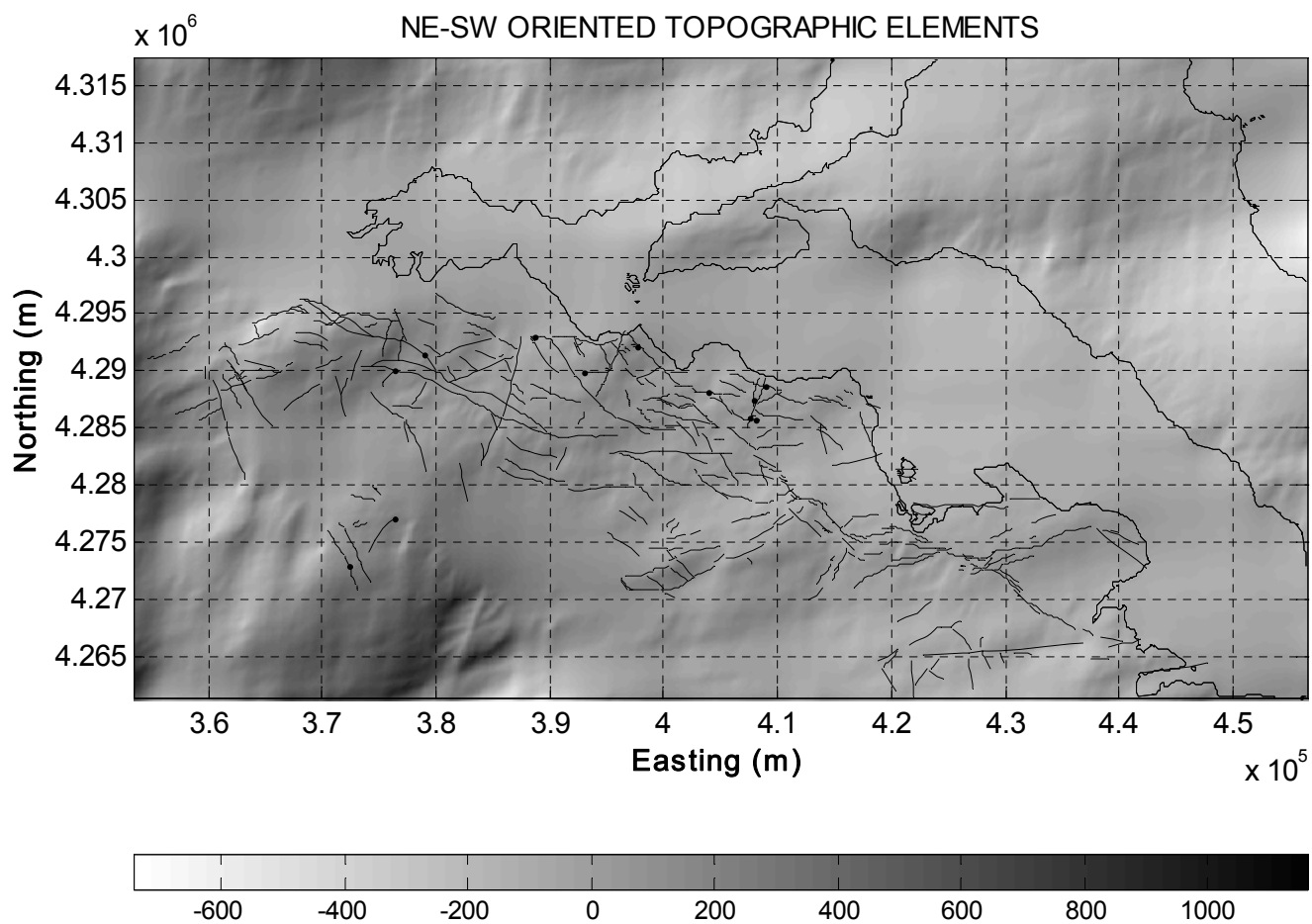


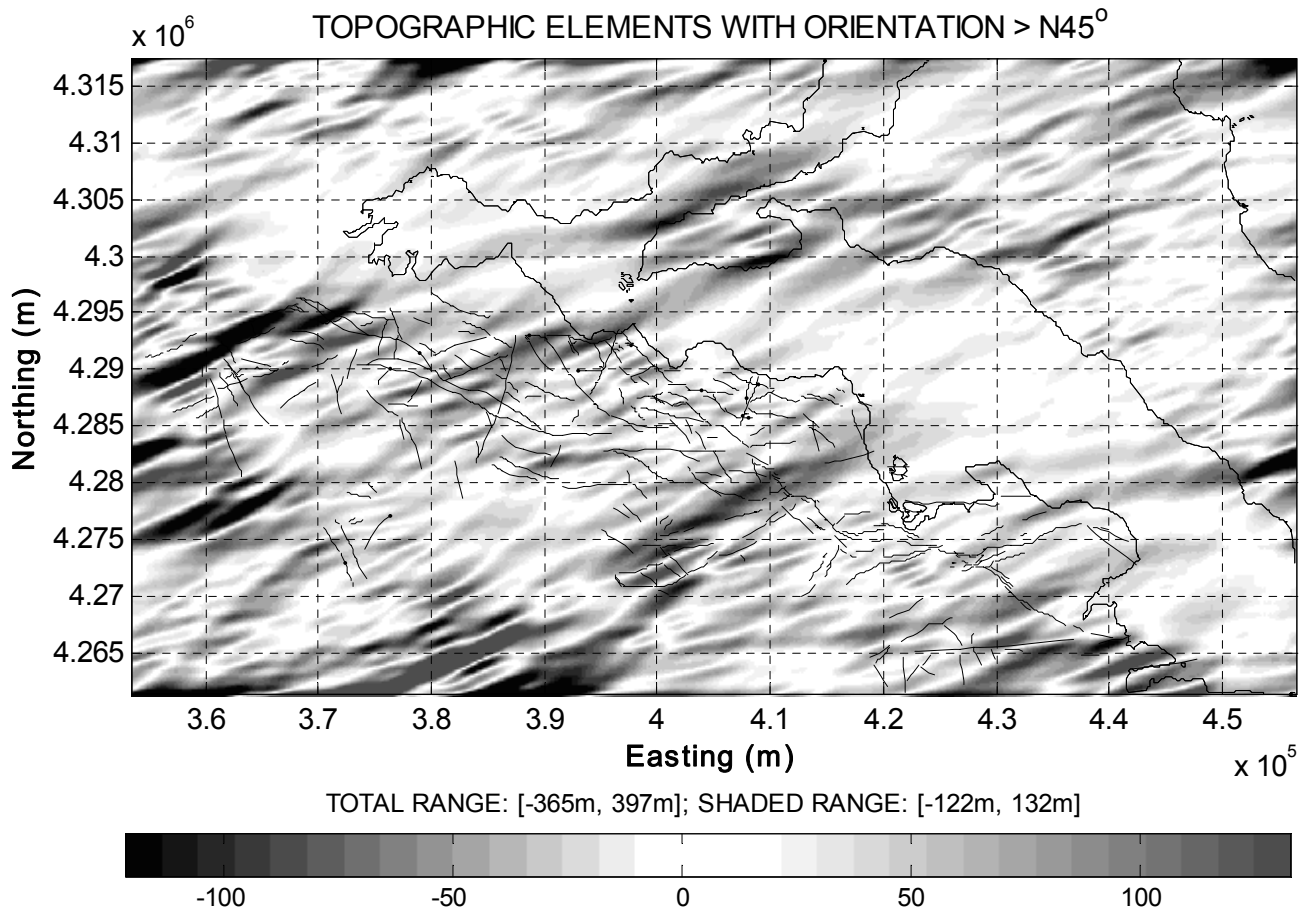
Accepte

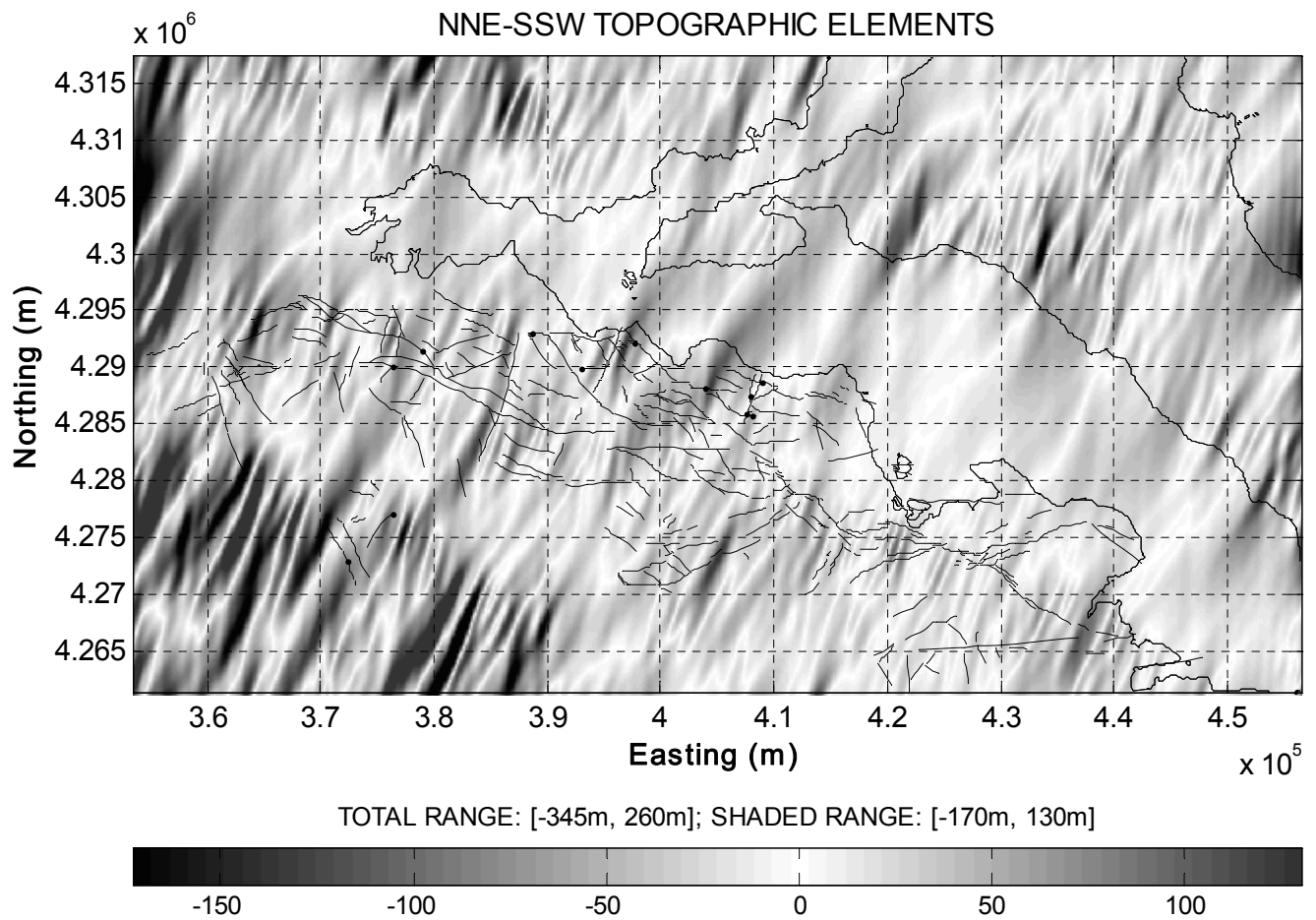


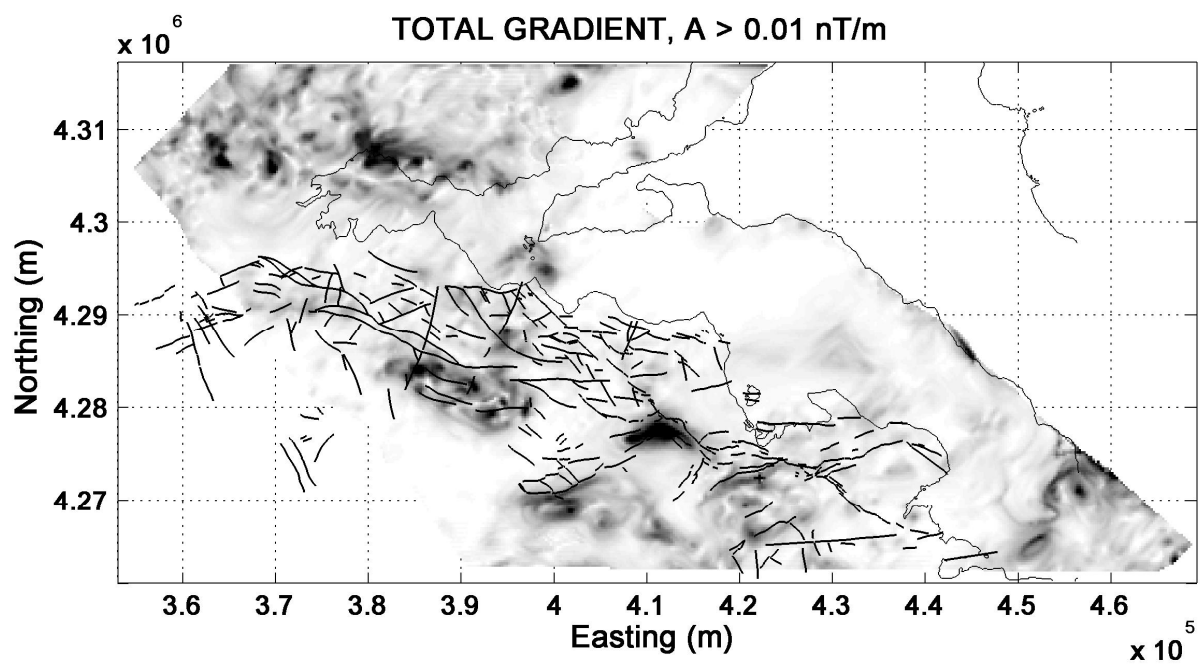
Accepte

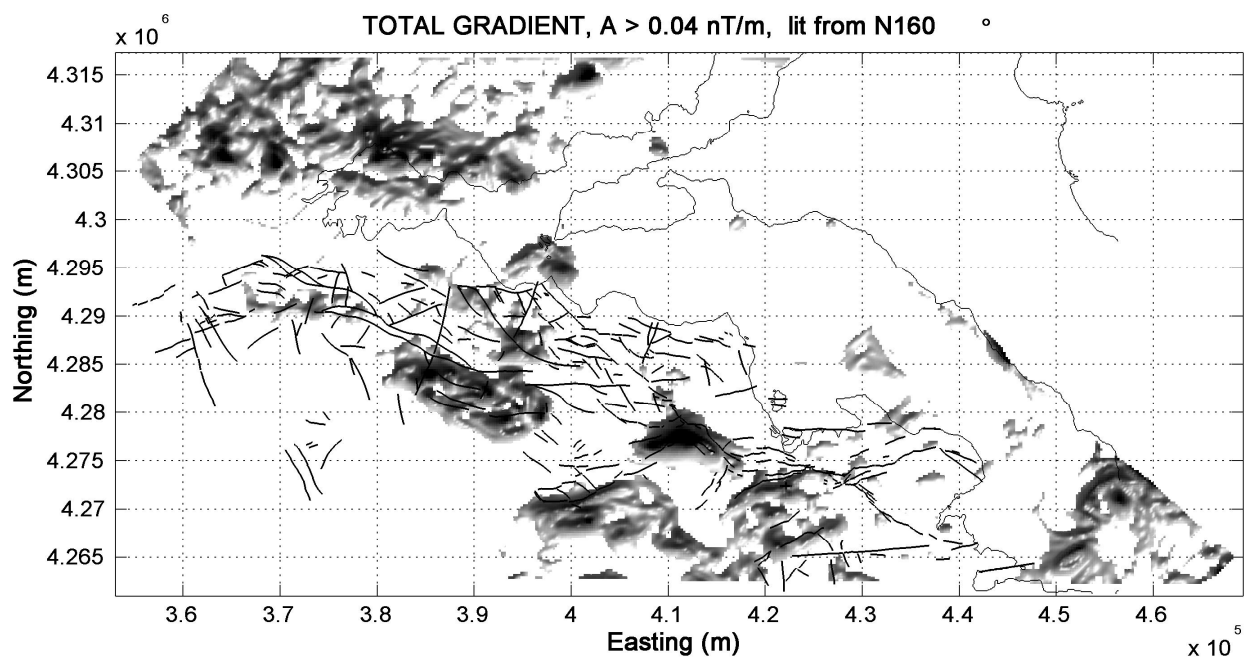


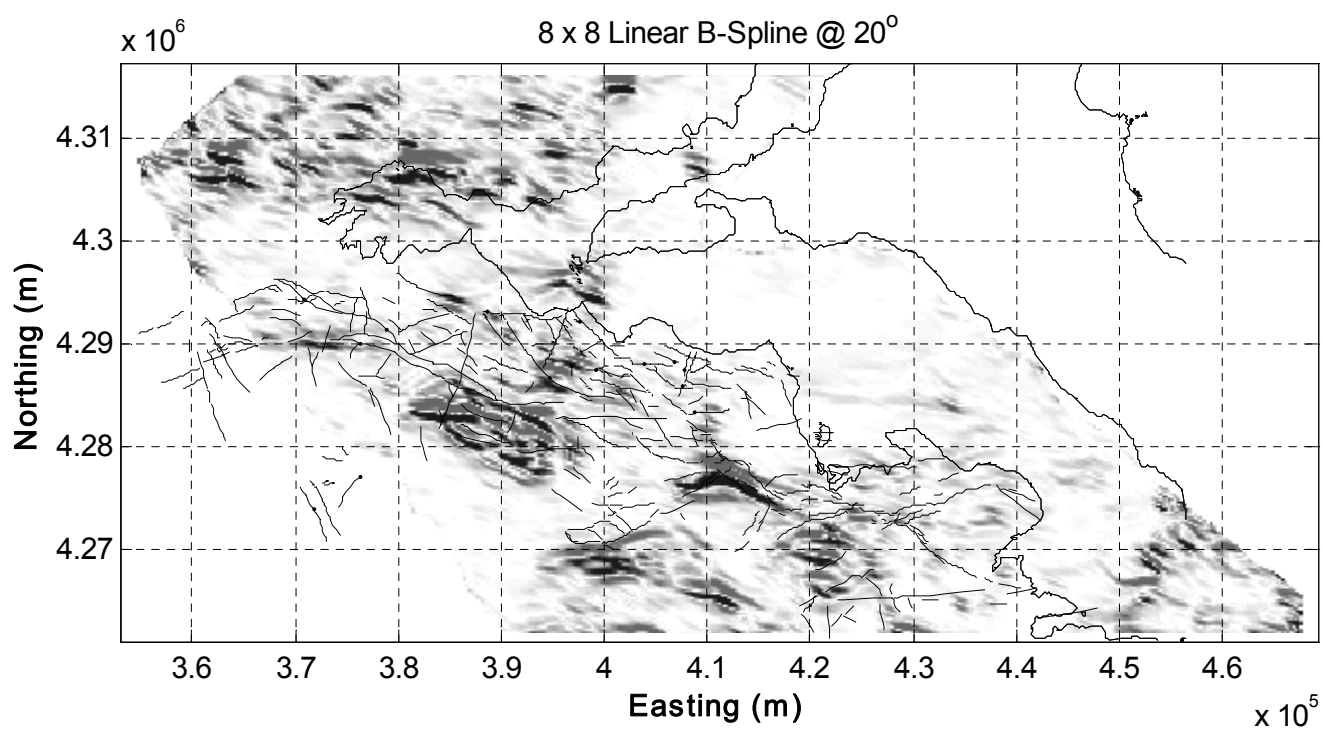












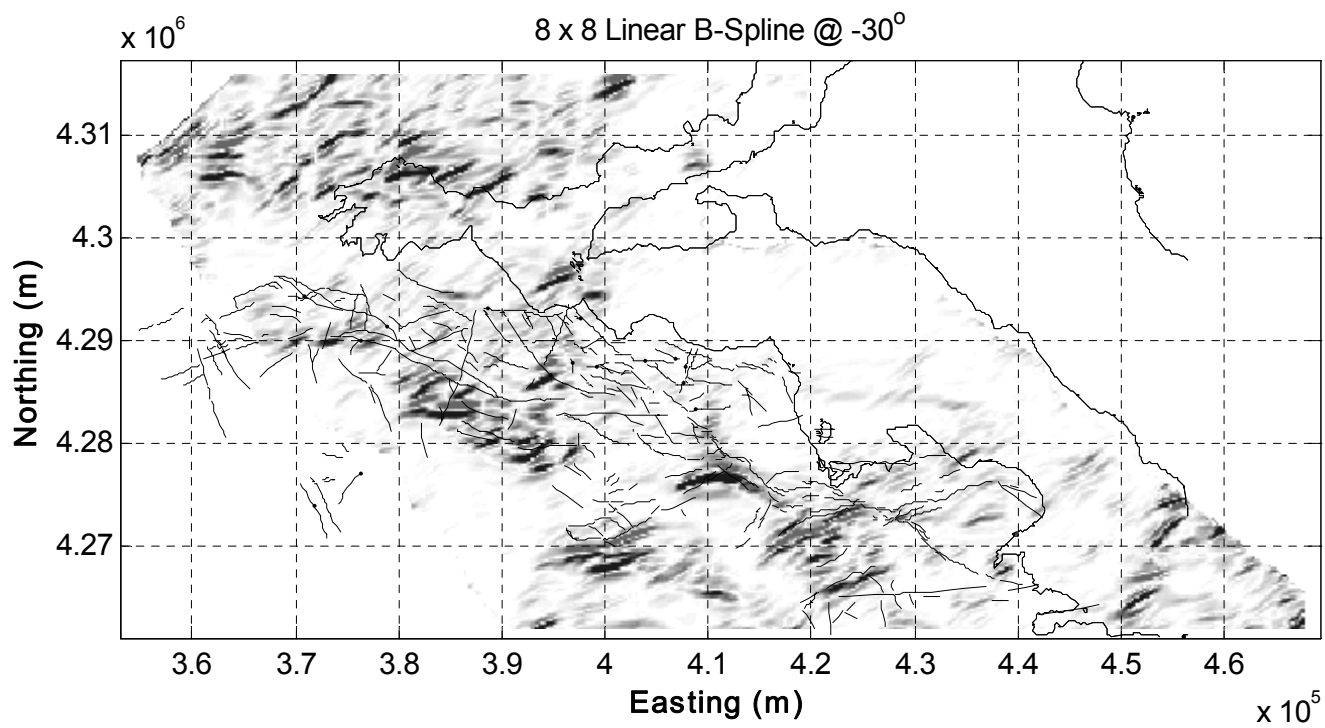


Figure 10

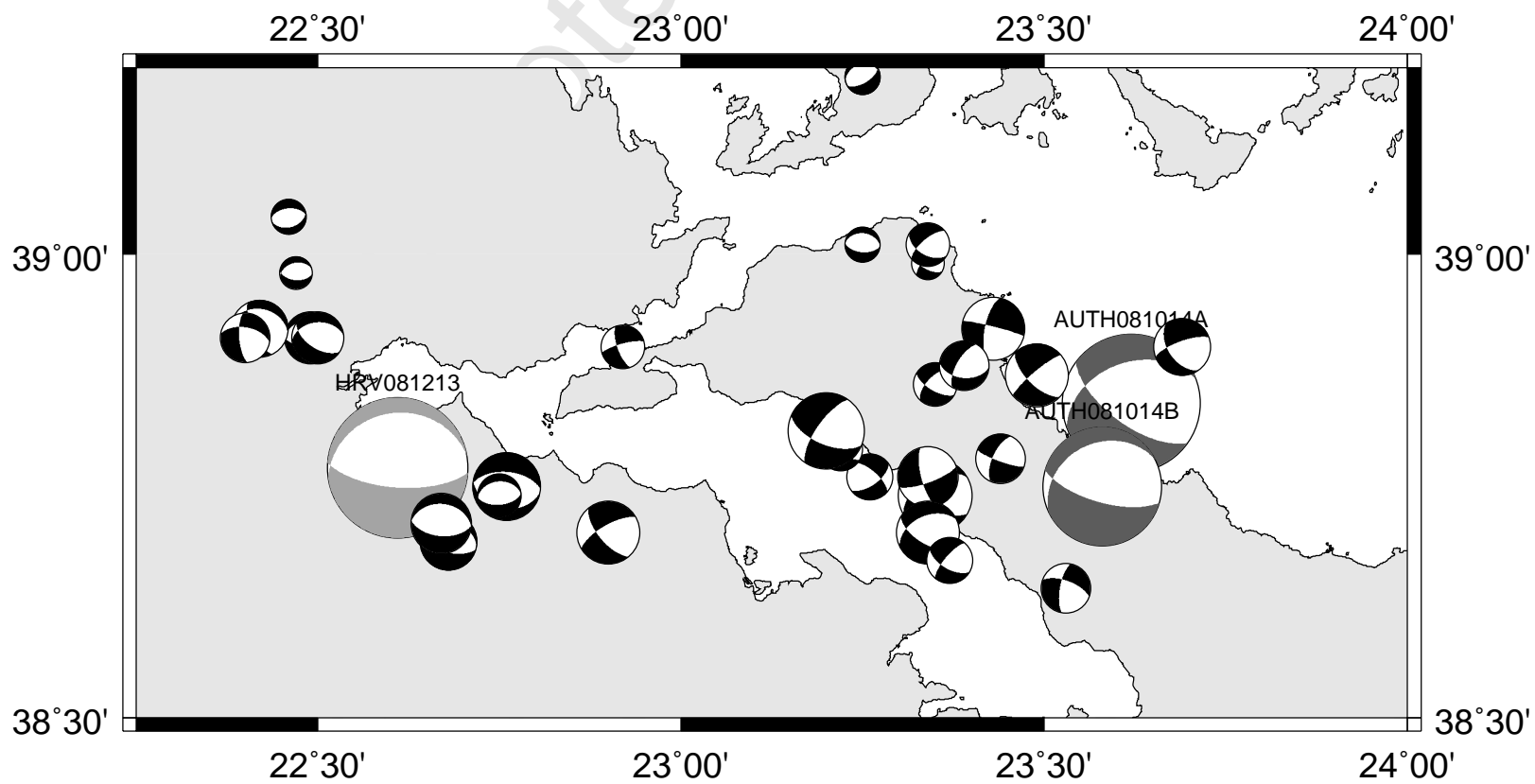
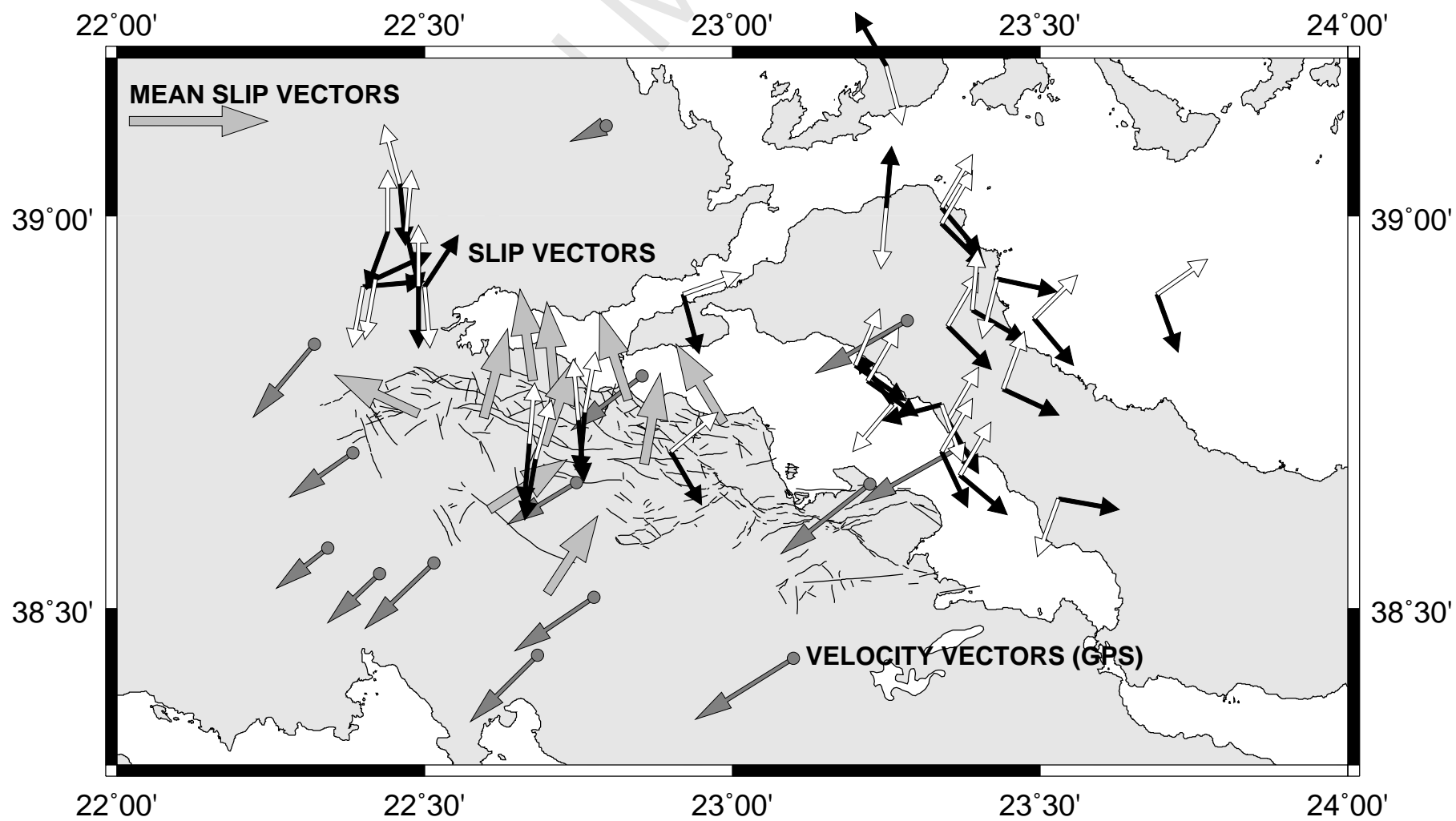
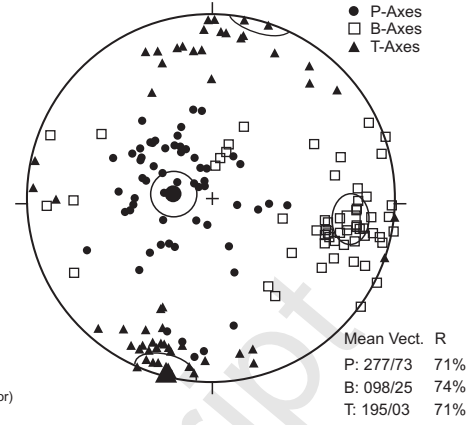
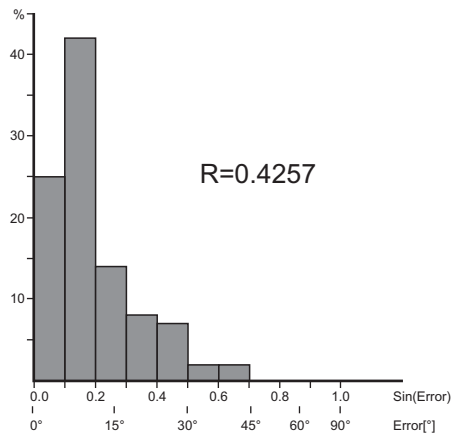
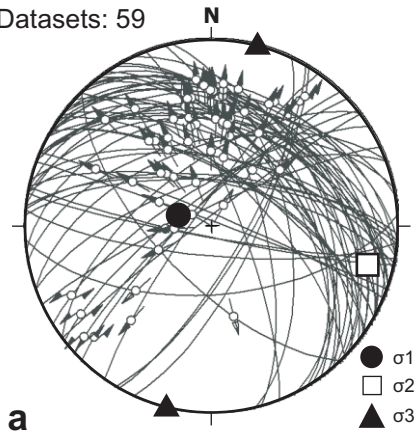


Figure 11



Coastal F.S.
Datasets: 59



Kallidromon F.Z.
Datasets: 29

